Complex Field Modulation in Direct Detection Systems

By

Kishanram Kaje

M.S., Polytechnic Institute of NYU, USA, 2010

B.E., Visveswaraya Technological University, India, 2008

Submitted to the graduate degree program in Department of Electrical Engineering and Computer Science and the Graduate Faculty of the University of Kansas in fulfillment of the requirements for the degree of Doctor of Philosophy

Chair: Rongqing Hui

Christopher Allen

Erik Perrins

Victor Frost

Jie Han

Date Defended: 12/11/2020

The Dissertation Committee for Kishanram Kaje certifies that this the approved version of following dissertation:

Complex Field Modulation in Direct Detection Systems

_____

Chairman: Dr. Rongqing Hui

Date Approved:12/11/2020

Abstract

Even though fiber optics communication provides a high bandwidth channel to achieve high-speed data transmission, there is still demand for higher spectral efficiency, faster data processing speeds with reduced resource requirements due to ever increasing data and media traffic. Also, lately the demand for online streaming because of remote working has increased significantly. Various multilevel modulation and demodulation techniques are used to improve spectral efficiency. Although spectral efficiency is improved, there are other challenges that arise. Such as requirements for high speed electronics, receiver sensitivity degradation, chromatic dispersion, operational flexibility, effects of nonlinearity impairments etc. Here, we investigate complex bandwidth efficient field modulation and coding techniques to improve spectral efficiency while reducing the digital signal processing (DSP) resources required for implementations using FPGAs or ASICs and compensation for linear and nonlinear impairments that appear in fiber optic communication systems. In this dissertation we investigated and developed solutions for various limitations and impairments in a direct-detection transmission system with complex field modulated optical signal. The solutions that we developed to compensate the fiber optical impairments can be implemented using DSP either at transmitter side or the receiver. By employing DSP based approach to mitigate the optical impairments and limitations we can achieve more flexibility in the optical transceivers while achieving higher spectral efficiency.

We proposed and demonstrated digital-analog hybrid subcarrier multiplexing (SCM) technique which can reduce the speed requirement of high-speed digital electronics such as ADC and DAC, while providing wideband capability, high spectral efficiency, operational flexibility and controllable data-rate granularity. Hybrid SCM is a modular approach in which multiple

digitally generated subcarriers are aggregated through RF oscillators and IQ mixers for frequency up- and down-conversions.

Next, to achieve maximum spectral efficiency with conventional Quadrature Phase Shift Keying (QPSK) we need highly spectral efficient Nyquist filters which require large amount of FPGA resources for digital signal processing (DSP). Hence, we investigated Quadrature Duobinary (QDB) modulation as a solution to reduce the FPGA resources required for DSP while achieving spectral efficiency of 2bits/s/Hz. We compared QDB with QPSK in a digital-analog hybrid subcarrier multiplexing system and we show that with minor changes in transmitter design we can achieve 2bits/s/Hz spectral efficiency, which is same as the Nyquist QPSK with relaxed resource requirements for DSP.

We investigated and developed a solution to digitally compensate the nonlinearities introduced by semiconductor optical amplifiers (SOA). In a field modulated direct-detection system, due to square-law detection of the photodiode, leads to an interference called signal-signal beat interference (SSBI). To eliminate SSBI we can use Kramers-Kronig (KK) receiver as we can retrieve the phase information from the direct detected optical signal for the class of signals called as minimum phase signals. However, it is under the assumption that the entire transfer function of our optical transmission system is linear except for photodiode. However, when the system transfer function is non-linear due to SOA nonlinearities when operated in gain saturation region. By using electrical forward propagation method for pre-compensation of nonlinearities caused by SOA we show that we can simultaneously restore the efficiency of KK receiver and as well achieve electronic dispersion post-compensation.

Acknowledgments

Firstly, I would like to express my heartfelt gratitude to my advisor Dr. Rongqing Hui for guiding me in the right direction, effectively helping me in successfully accomplishing this dissertation thesis. Dr. Hui, has influenced me in multiple ways to mold my thinking style, improving my problem-solving skills and communicating the information in effective and impactful way.

Also, my sincere thanks to Dr. Erik Perrins, Dr. Christopher Allen, Dr. James Stiles, Dr. Victor Frost for their excellent lectures that tailored my mathematical and analytical skill levels in comprehending and analyzing communication systems and signal processing algorithms.

My sincere thanks to Dr. Jie Han for accepting my request to be on my dissertation committee.

Lastly, I would like to express my heartfelt gratitude to my parents, sister and my wife for the encouragement and support in all ways during the time of my graduate studies at The University of Kansas.

Table of Contents

Chapter 1: Introduction & Literature Review 1

1.1 Motivation & Background 1

1.2 Coherent Detection Systems 3

1.3 Direct Detection Systems 4

1.4 Overview of the research work 5

1.2.1 Digital Analog Hybrid Subcarrier Multiplexing (SCM) 5

1.2.2 Reduce DSP resources for filters using QDB 5

1.2.3 Digital compensation for SOA nonlinearities in Kramers-Kronig DD system 7

Chapter 2: Digital Analog Hybrid Subcarrier Multiplexing 10

2.1 Introduction 10

2.2 Hybrid SCM Transceiver Architecture 11

2.3 Experimental Configuration and Results of Measurements 13

2.4 Detection with a high-speed receiver 17

2.5 Detection with narrowband receiver 20

2.6 Conclusion 22

Chapter 3: QDB Modulation to reduce DSP resource requirement 24

3.1 Introduction 24

3.2 Duobinary Coding 25

3.3 Quadrature Duobinary Modulation 27

3.4 OSNR requirement and resource estimation 31

3.5 Experimental Configuration 33

3.6 Simulation and Experimental Results 35

3.7 Sensitivity recovery possible using MLSE 40

3.8 Conclusion 42

Chapter 4: Digital pre-compensation of SOA nonlinearities in field modulated direct-detection systems 43

4.1 Introduction 43

4.2 Kramers-Kronig Receiver 45

4.3 SOA impairments and compensation 46

4.4 Experimental Setup 48

4.5 Experimental Results and Discussion 51

4.6 Conclusions 55

Future Work 56

REFERENCES 57

List of Figures

Figure 1:Generic Coherent Detection System 3

Figure 2:Generic Direct Detection System 4

Figure 3: Block diagram of a hybrid SCM Transceiver. HYB: 90° hybrid. 12

Figure 4: Test-bed of a hybrid SCM system with 3 RF subcarriers 14

Figure 5: Double-sideband RF spectrum 14

Figure 6: Single sideband RF spectrum 14

Figure 7:Schematics of IQ mixing without a 2x2 90° hybrid 15

Figure 8:Schematics of IQ mixing with a 2x2 90° hybrid 16

Figure 9:Single sideband optical spectrum 17

Figure 10:Two double-sideband RF subcarriers at 5GHz and 7.2GHz, each carrying I and Q channels. (a) spectrum measured with a high-speed receiver. (b) EVM of recovered digital subcarrier channels 18

Figure 11: Two single-sideband RF subcarriers at 5GHz and 7.2GHz, each carrying an I or Q channel. (a) spectra measured with a high-speed receiver. (b) EVM of recovered digital subcarrier channels 19

Figure 12:(a) block diagram of frequency down-conversion using based on IQ mixing in the receiver, (b) spectra of recovered I and Q channels on the 7.2GHz RF carrier, and (c) measured EVM of I and Q channels 20

Figure 13: (a) and (b) spectra of recovered I and Q channels on the 7.2GHz RF carrier with SSB modulation, and (c) measured EVM of I and Q channels 21

Figure 14: Duobinary signal generation using a one-tap delay and add filter 25

Figure 15: Spectral shaping comparison between binary and duobinary signals, most of the required spectrum for demodulation is under shaded section. 26

Figure 16: Block diagram to generate Quadrature Duobinary Signal. 28

Figure 17: Transfer function of the Nyquist Filter used for QPSK spectral shaping 30

Figure 18: Transfer function of the Nyquist Filter used for QDB spectral shaping 30

Figure 19:Experimental setup to transmit and receive QDB and QPSK signals (AWG: Arbitrary waveform generator) 33

Figure 20: Received spectrum of QPSK(a) and QDB(b) 34

Figure 21: EVM vs beta for QPSK-FDM 36

Figure 22: EVM vs beta for QDB-FDM 37

Figure 23: EVM vs SNR for QPSK-FDM using Equation 5 38

Figure 24: EVM vs SNR for QPSK-FDM using equation 6 38

Figure 25: EVM vs SNR for QDB-FDM using equation 6 39

Figure 26: Experimental EVM vs beta for QPSK-FDM 39

Figure 27:Experimental EVM vs beta for QDB-FDM 40

Figure 28: Trellis for MLSE detection for QDB 41

Figure 29: KK direct detection: CW is added at the left of the signal spectrum with bandwidth B 45

Figure 30: Experimental SOA gain characteristics 47

Figure 31: Experimental set up. Wavelogic Ai has the ability of selecting the output optical power, and to adjust the saturation level of the SOA or external variable optical attenuator can be used. 48

Figure 32: Single sideband modulated Optical Spectrum 49

Figure 33: Received RF spectrum of 14G baud QAM16 signal..... 50

Figure 34:Experimental EVM vs CSPR plots for back to back setup and with fiber when SOA is operated in linear region (line with stars, line with squares) and nonlinear region with pre-compensation (line with diamonds, line with circles) 51

Figure 35:(a) and (b) shows simulation results of BER versus OSNR for back to back and with fiber dispersion..... 52

Figure 36:Experimental data showing BER Vs OSNR plots for back to back setup. CSPR of 11dB. Insets (i), (ii), (iii) shows typical constellation diagram of received QAM-16 signal when SOA is operated in linear region, nonlinear region with and without pre-compensation for impairments respectively 53

Figure 37:Experimental data showing BER vs OSNR for the case when 78.28km fiber was included. CSPR of 11dB 54

List of Tables

Table I. RESOURCE ESTIMATION AND UTILIZATION 33

Table II. ADDITIONAL RESOURCES NEEDED FOR MLSE 41

Page left blank intentionally

Chapter 1: Introduction & Literature Review

1.1 Motivation & Background

Although fiber optic networks are capable of high-speed data transfer, there is still very high demand for even faster speeds due to rapid increase in data, media traffic. According to Cisco report the global IP traffic will grow three-fold from 2017 to 2022, making it grow at compounded rate of 26%. IP traffic will reach 396 Exabytes (EB) per month by 2022, up from 122.4 EB per month in 2017 [50]. There will be 3.6 networked devices per capita by 2023, up from 2.4 networked devices per capita in 2018. There will be 29.3 billion networked devices by 2023, up from 18.4 billion in 2018 [40]. There will be nearly 5.3 billion total Internet users by 2023, that is 66% of global population. The share of Machine-To-Machine (M2M) connections, things like connected home and car applications, will grow from 33 percent in 2018 to 50 percent by 2023 [40]. There will be 14.7 billion M2M connections by 2023 [40]. Over 70 percent of the global population will have mobile connectivity by 2023. Now, this leads to increase in demand for higher data rates, which in turn puts huge request on optical transport networks for higher transmission capacities. To accommodate this continuous call for higher data rates we need to make sure the present optical networks are put to use as efficiently as possible. As result of necessity to improve the existing optical networks, flexible optical transceivers have made way to the rise.

Optical transceiver flexibility can be achieved in multiple ways such as adopting higher order multilevel modulation formats, increasing the symbol rate, increasing the number of subcarriers. To achieve better transmission reach adjusting the ratio of forward error correction to payload, reduce the gap between optical subcarriers, reduce the guard band between super-channels allotted by The International Telecommunication Union Telecommunication Standardization Sector (ITU-

T) fixed 50 GHz grid wavelength allocation plan. ITU-T plan can accommodate 80 channels [61]. More the degrees of flexibility are accommodated in an optical transceiver, better the performance of the optical network in accommodating the data traffic. However, being practical we cannot have it all as we need to take in to consideration of increased complexity and impact of cost in implementation. Regardless of flexibility provided by an optical transceiver, when an optical signal passes through an optical transmission system it has to survive various transmission impairments. This creates demand for more research on these optical transmission systems to improve data rates, provide finer data granularity, better resource allocation in digital signal processing and more.

In fiber optic communications, signal-controlled element exhibiting the electro-optic effect is used to modulate laser light. The modulation is applied on the phase, amplitude, or polarization of the beam. Amplitude or intensity modulation (IM) is one of the most commonly used modulation is when data is modulated as a function of intensity of the carrier. ON-OFF Keying (OOK), PAM4, NRZ are some of the IM techniques. On the other hand, phase modulation is where instantaneous phase of the carrier is encoded with modulation pattern. Commonly used phase modulation schemes are QPSK, 8-PSK etc. The receiver systems can be categorized as direct detection (DD) receivers and coherent detection receiver systems. Coherent detection receivers, a type of receivers where phase of the incoming optical signal is recovered. Although, coherent receivers provide better receiver sensitivity and retains phase information of the optical signal, they're known for highly complex implementation which in turn is not budget friendly. On the other hand, DD receivers are simple intensity detection receivers where received optical signal is fed to a photodetector (PD) which in turn converts the optical signal into electric current according to square law detection. Regardless of the type of receiver systems used in an optical communication,

as the signal passes through the entire transmission and receiver system, it goes through several number of impairments both linear and nonlinear due to optical devices and optical fibers used. Some of the impairments are laser phase noise, frequency chirp, non-perfect sideband suppression at the modulator, amplified spontaneous emission (ASE) noise from optical amplifiers, nonlinear effects in certain semiconductor optical amplifiers, fiber attenuation and chromatic dispersion from optical fiber, signal-signal beat interference in direct detection receiver and so on.

1.2 Coherent Detection Systems

Figure 1 below shows the generic block diagram of coherent detection system. Coherent detection originally is based from radio communications, where a local oscillator is used to mix with the received RF signal to generate a product term [19]. In optical systems, although operating principle is similar to RF systems fundamentally, the operating frequency is obviously much higher than the radio frequencies. In coherent detection systems, the data can be modulated onto the phase of the carrier along with the magnitude using external modulator. In coherent detection, the photocurrent is proportional to the field of the optical signal. Hence the phase information of the optical signal is preserved. Homodyne detection and heterodyne detection configurations are different techniques used in coherent receivers [19] to recover the phase information. Regardless

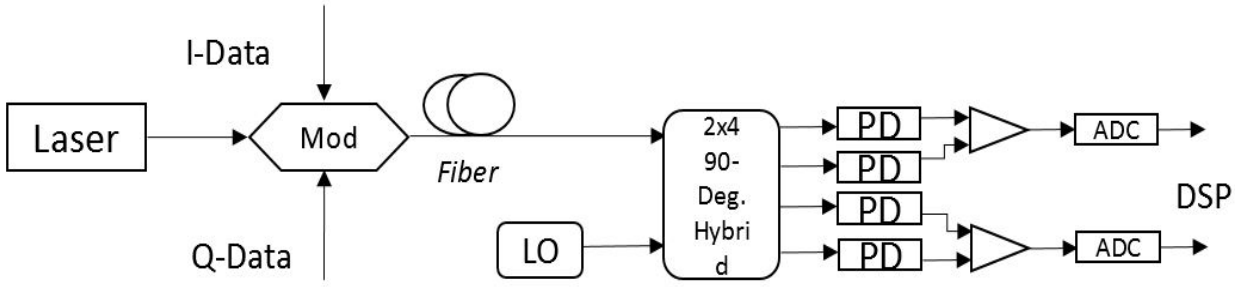

Figure 1:Generic Coherent Detection System

of the type of detection technique is used, coherent receivers are complex to implement and are not so cost effective.

1.3 Direct Detection Systems

Generic architecture of a typical direct detection system is shown in Figure 2 below. In direct detection systems the data is retrieved from an optical signal using a simple photodetector diode (PD) which will convert the optical intensity in to an electric current using square law detection. That is the detection is based on optical power. The receiver usually consists of PD along with clock recovery and symbol decision module which could be done using digital signal processing (DSP). In comparison with coherent detection systems which use digital-to-analog converters (DACs), dual-polarization I/Q modulators, optical hybrids, multiple photodetectors and analog to digital converters (ADCs), DD systems use much more simple and affordable optics. They are a very attractive technology for short and medium reach optical fiber transmission systems. The DD systems are very attractive because it is less complex, requires low power consumption, size, budget friendly etc. Although DD systems suffer from chromatic dispersion (CD), most of the commercial optical links have dispersion compensation fibers (DCF) making DD systems a very good option. Recently field modulation in combination with direct detection receiver is getting a lot of attention. Also, there are works, where phase information could be retrieved in certain scenarios of direct detection transmission setups [56].

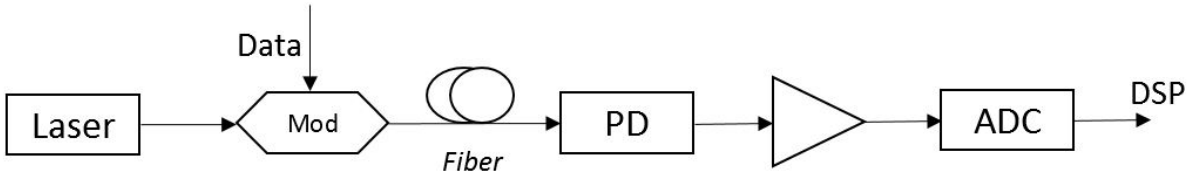

Figure 2:Generic Direct Detection System

1.4 Overview of the research work

Due to low cost and low complex implementation benefit of DD receivers, we employed this type of receiver system in our research. Traditionally intensity modulation is used at the transmitter side of the DD transmission systems. To improve data rate and hence spectral efficiency we adopt bandwidth efficient high order multilevel field modulation techniques at the transmitter side. However, this leads way to several impairments in the transmission system resulting in degradation of the performance.

This dissertation is a compilation of applied research where we proposed and developed DSP based solutions to mitigate impairments and limitations in a complex field modulated direct detection transmission system while improving spectral efficiency. As we all know, there has been tremendous increase in the capacity of DSP processing power in recent years. This helps us to adopt our proposed solutions in digital domain for an existing optical transport network. The added flexibility to improve the existing optical transmission systems in digital domain without the need to spend money on expensive optical hardware makes the proposed solutions very convenient and budget friendly.

This research work includes three major topics where we show different DSP techniques to improve the flexibility of an optical transmission system and are as follows.

1.4.1 Digital Analog Hybrid Subcarrier Multiplexing (SCM)

Internet Protocol (IP) routers are used to achieve efficient statistical multiplexing of the available network resources [1, 2]. However, it is an expensive solution because of the requirement of dynamic packet processing including power hungry forward engine, buffering and routing. Circuit-switched optical networks have the potential to provide end-to-end dedicated circuits

between edge node pairs without the need of processing in the packet level [3, 4]. Due to continuous demand of media content in the internet, as well as latency-sensitive applications such as online gaming, tele-surgery, high frequency trading to name a few, circuit-based network architecture may provide a better solution [33]. Nevertheless, data rate flexibility and the efficiency of resources sharing between users have to be significantly improved before circuit switch-based optical networks can be widely adopted for practical applications.

It is popularly known that wavelength routed transparent network architecture can reduce the need for electrical regeneration and reduce the cost. Spectrum-sliced elastic optical path network (SLICE) with flexible-grid developed in recent years [5, 6] provides improved bandwidth granularity in comparison to traditional WDM-based and wavelength-routed optical path networks. This helps address flexible capacity requirement of next generation dynamic optical networks. However, data-rate granularity of spectrum-slicing in the optical domain based on wavelength-selective switch (WSS) is limited by frequency selectivity of optical filters, which is often not fine enough for efficient resource sharing between end users. Digital subcarrier multiplexing (DSCM) [7] in electrical domain is able to adopt bandwidth efficient modulation formats and provide much finer data rate granularity and flexibility for circuit-based networking. But to accommodate the increase of bandwidth carried by each wavelength, the speed of digital electronics such as analog-to-digital converter (ADC) and digital-to-analog converter (DAC), has to be increasingly higher. Although high-end ADC and DAC with sampling rates at or higher than 56GS/s are commercially available for major telecom equipment manufacturers [8], the analog bandwidth of these devices is still lower than the available bandwidths of electro-optic modulators, photodetectors and RF amplifiers.

In this research work, we proposed and demonstrated the digital-analog hybrid SCM technique to reduce the requirement for high speed digital electronics while providing, wide band capability, controllable data-rate granularity, high spectral efficiency and operational flexibility. Taking advantage of both digital flexibility and broadband capabilities of RF circuits, this hybrid structural approach allows the scaling to data rates without the need for high speed ADC and DAC. This work is elaborated in Chapter 2 of this dissertation.

1.4.2 Reduce DSP resources for filters using QDB

For implementing highly spectral efficient digital subcarrier multiplexing (DSCM) scheme like Quadrature Phase Shift Keying (QPSK) frequency division multiplexing (FDM) we would need to perform spectral shaping so that there is minimum inter-channel crosstalk and inter-symbol interference. The spectral shaping of individual QPSK subcarrier channels in QPSK-FDM can be done using Nyquist filters with very sharp roll-off factor. However, in order to realize these filters on FPGAs or ASICs we need to take in to consideration of DSP resources required to implement. This is because of limited DSP resources available on FPGAs or ASICs.

In this work, we for the first time used quadrature duobinary coding in digital domain to significantly reduce the overall FPGA resources required for digital signal processing (DSP) in a frequency-division multiplexed (FDM) optical system while achieving 2bit/s/Hz spectral efficiency [32]. With conventional quadrature phased shift keying (QPSK) scheme, an ideal Nyquist filter with sharp edges has to be used to achieve 2bits/s/Hz spectral efficiency, and the high order digital filter requires tremendous resources in implementation using FPGA. The high spectral concentration of Quadrature Duobinary (QDB) coding greatly relaxes the requirement on the filter frequency selectivity, allowing FIR filter with much lower order to be used to achieve the same spectral efficiency. We compared the performance of QDB with QPSK and we show that

with minor changes in transmitter design, 2bit/s/Hz spectral efficiency can be achieved with much reduced resource requirement for digital signal processing [32]. More details on this work is explained in Chapter 3 of this dissertation.

1.4.3 Digital compensation for SOA nonlinearities in Kramers-Kronig DD system

In complex field modulated direct detection optical systems, due to square law detection it is required to provide a guard band to avoid signal-signal beat interference (SSBI). The required guard band is equal to the signal bandwidth (B). This method is very inefficient considering a loss of 50% spectral efficiency. Also, when an optical signal travels along an optical fiber, apart from signal power being attenuated, the different frequency components within the signal travel at slightly different speeds [19]. This type of propagation which is frequency dependent is called as chromatic dispersion. We cannot compensate for fiber dispersion digitally in a direct detection system. To mitigate both of these problems, we can use Kramers-Kronig (KK) receiver [56] after photodetection. KK algorithm can recover phase information of an optical signal from the intensity for a class of signals called as minimum phase signals. To successfully mitigate SSBI and compensate for fiber chromatic dispersion in digital domain after KK receiver we need a transmission system with linear transfer function before photodetection. If the transmission system has nonlinear impairments KK receiver performance would be inaccurate.

In this research work, we investigated and developed solution to mitigate nonlinear impairments in complex field modulated transmission systems with integrable semi-conductor optical amplifiers (SOA). SOAs are one of the very attractive solutions for optical amplification. However, SOAs come with its own limitations. When operated at lower input powers SOAs work in linear region, however, when we increase the input power then SOA introduces nonlinearities due to gain saturation. This in turn makes compensation of SSBI and chromatic dispersion

inaccurate after KK detection. These nonlinearities can be digitally compensated using backpropagation method [54] in an intensity modulation direct detection system. However, it is not possible in direct detection systems when it is field modulated. We developed a method to compensate for nonlinearities due to SOA operating in gain saturation in a field modulated KK receiver system, which in turn can successfully mitigate SSBI and fiber chromatic dispersion digitally. More details on this work with results of simulation and experiments is shown in Chapter 4 of this dissertation.

Chapter 2: Digital Analog Hybrid Subcarrier Multiplexing

2.1 Introduction

Subcarrier multiplexing (SCM) has been used for optical transmission, in which high speed data is partitioned into multiple subcarrier channels [9]. The spectral efficiency of traditional analog-based SCM is relatively low due to the requirement of spectral guard-band between subcarrier channels. With the advancements in microwave/RF technology, Nyquist filters can be designed to shape the RF spectrum so that spectral guard-band can be reduced and the efficiency of SCM can be improved [10]. However, in comparison to digital electronics, analog RF circuits still lack flexibility and controllability to adapt dynamically varying network requirements.

In this chapter, we demonstrate a digital-analog hybrid subcarrier multiplexing (hybrid-SCM) technique to increase the bandwidth carried by each wavelength but while reducing the requirement on the speed of digital electronics such as ADC and DAC. Hybrid-SCM is a modular approach in which multiple digitally generated subcarriers are aggregated through RF oscillators and IQ mixers for frequency up conversion in the transmitter and down conversion in the receiver. While digital electronic processing provides high level flexibility for software controllable and spectrally efficient modulation, RF multiplexing/demultiplexing allows the scale-up of per-wavelength traffic capacity. Thanks to the rapid development of 5G wireless systems into the millimeter-wave region, high quality RF oscillators and mixers are readily available with low power consumption and reduced cost. Precise frequency control and phase locking of RF oscillators allow RF subcarrier channels to be tightly packed without the guard band so that the spectral efficiency is not compromised. The ability of individually addressing the data rate and the modulation format of each subcarrier channel provides extraordinary flexibility for network design and operation. More importantly, as each RF subcarrier channel can be turned-on or powered-off

depending on the network status and dynamic bandwidth requirement [11], power saving can be achieved in comparison to using a single high-speed ADC or DAC.

2.2 Hybrid SCM Transceiver Architecture

The basic block diagram of a hybrid-SCM transceiver is shown in Figure 3. A number of subcarrier channels are digitally generated and up-loaded onto RF subcarrier frequencies $f_1, f_2,...f_M$ through mixing with RF local oscillators. The ability of frequency control and phase locking of RF oscillators allow RF subcarrier channels to be tightly packed without the need of guard-band so that high spectral efficiency can be achieved. Inphase-quadrature (IQ) mixing allows coherent frequency up-conversion, in which positive and negative sidebands of each RF subcarrier can be used to carry independent data channels C_i and D_i with $i = 1...M$. These RF subcarrier channels are aggregated into a composite electric waveform, which is then converted into an optical signal through electrical-to-optical (E/O) conversion using an electro-optic modulator.

This modularized parallel approach utilizing multiple RF subcarriers allows the increase of total traffic bandwidth on each wavelength without increasing the speed of digital electronics. Since each RF subcarrier channel is created digitally, it can be composed of multiple digital subcarriers, which provides an additional level of flexibility in data rate granularity.

In the receiver side, both direct detection and coherent detection can be used for optical-to-electrical (O/E) conversion. Each RF subcarrier channel can be frequency down-converted into baseband through an RF local oscillator and an IQ mixer. This baseband signal is then digitized by an ADC and processed to recover data traffic carried on that subcarrier. If a high-speed ADC is available, it is also convenient to digitize the composite electrical waveform directly after photo-

detection, and perform frequency down-conversion of various RF subcarrier channels through digital processing.

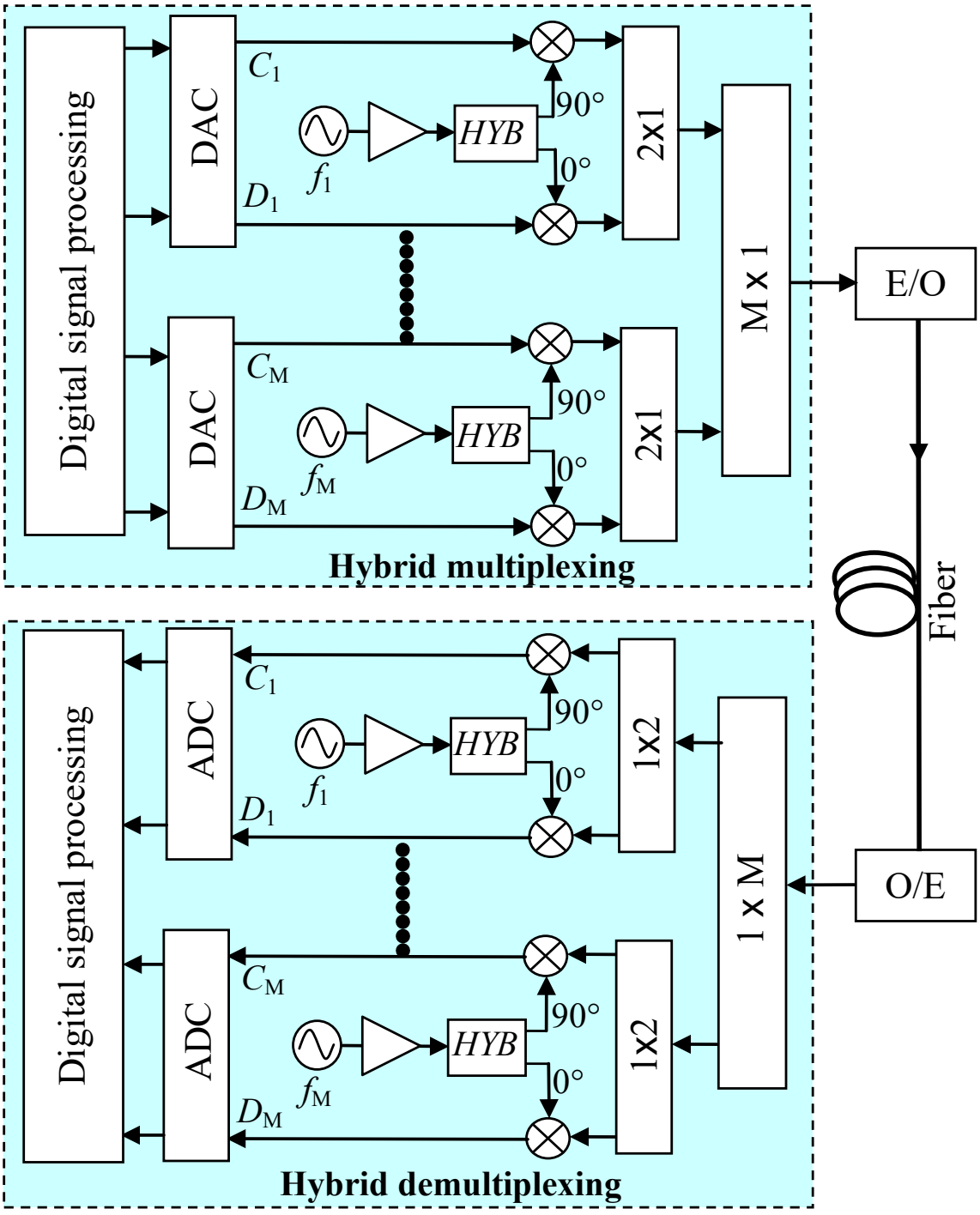

Figure 3: Block diagram of a hybrid SCM Transceiver. HYB: 90° hybrid.

Both orthogonal frequency-division multiplexing (OFDM) [12, 13] and Nyquist frequency-division multiplexing (Nyquist-FDM) [14, 15] can be used to generate digital subcarriers with high spectral efficiency and controllable spectral shape. However, the separation of adjacent OFDM subcarrier channels relies on the data phase synchronization between them so that integration can be performed precisely within the duration of a bit. On the other hand, channel selection of Nyquist-FDM relies on Nyquist filtering in the frequency domain, so that phase synchronization between subcarrier channels in the time domain is not required. Thus, from a dynamic network point of view, Nyquist-FDM appears more suitable to handle largely asynchronous data traffics carried by different subcarriers.

2.3 Experimental Configuration and Results of Measurements

Figure 4 shows the experiment setup used to test a hybrid-SCM system. In this example, 4 RF subcarriers are used at frequencies of 1GHz, 3GHz, 5GHz and 7GHz, with 2GHz full bandwidth carried by each RF subcarrier. Figure 5 and 6 show the measured RF spectra, where spectra of different colors represent subcarrier channels when they are turned on individually. In Figure 5 each subcarrier channel has double sidebands with each sideband carrying an independent data channel, whereas in Figure 6 only a single sideband is turned-on for each subcarrier so that the rejection of the opposite sideband can be evaluated.

IQ mixing is a technique commonly used in coherent RF systems in which the two modulation sidebands of an RF carrier are not redundant so that they can be used to carry independent data channels. In this setup, although the overall bandwidth is 8GHz, the required analog bandwidth of digital electronics such as DAC and ADC is only 1GHz. More importantly, each subcarrier channel can be turned on and off independently depending on the dynamic bandwidth demand of the network.

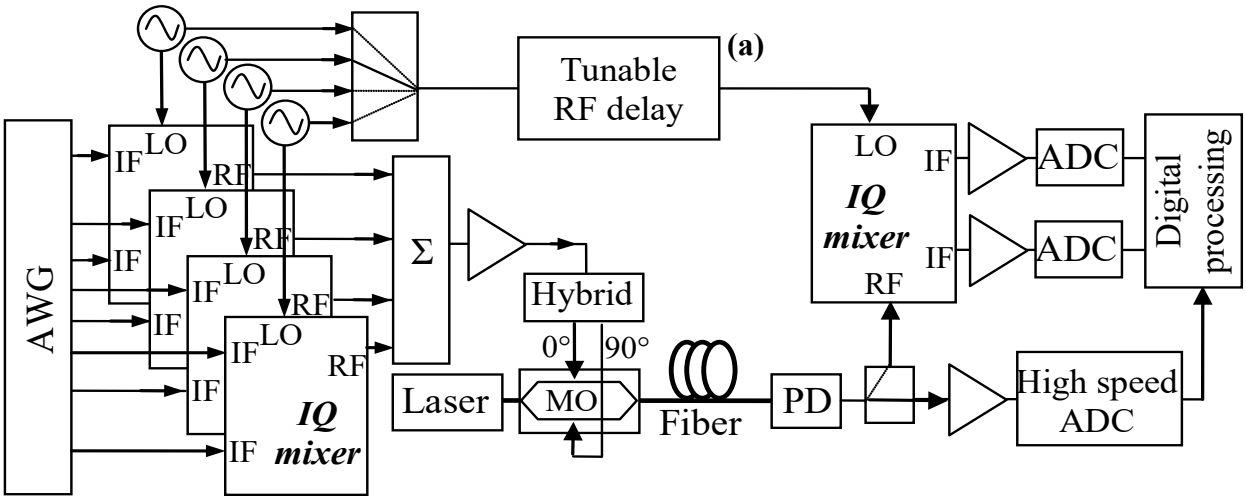

Figure 4: Test-bed of a hybrid SCM system with 3 RF subcarriers

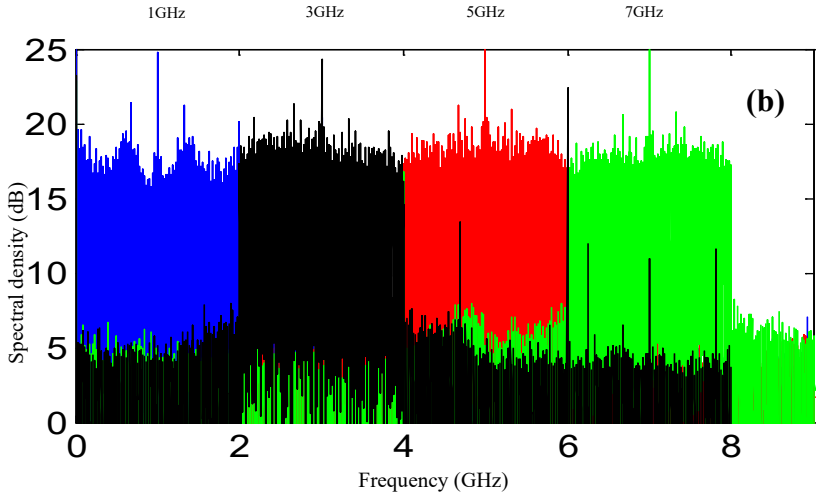

Figure 5: Double-sideband RF spectrum

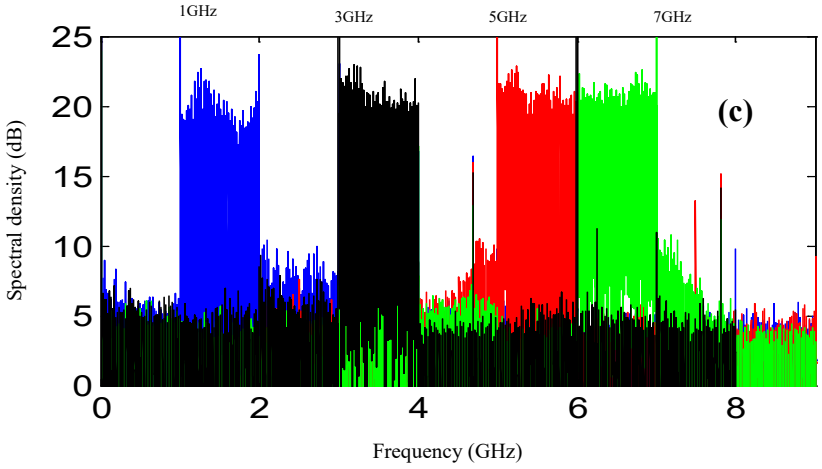

Figure 6: Single sideband RF spectrum

In a basic RF up-conversion configuration based on IQ mixing, the inphase (*I*) and the quadrature (*Q*) channels are mixed with the sine and the cosine components of the RF carrier independently before they are combined as shown in Figure 7. To avoid spectral overlap, the minimum frequency of the RF carrier, f_i, is equal to half of the full bandwidth of the *I* and the *Q* channels. In this case, the upper and the lower sidebands of the up-converted complex RF spectrum carry *I*+*jQ* and *I*-*jQ*, respectively, so that the *I* and the *Q* channels can be separated in the receiver by IQ demultiplexing. However, the *I* and the *Q* channels are not spectrally separated in the up-converted RF spectrum, and the quality of IQ mixing including sideband suppression ratio and power equalization cannot be directly evaluated before frequency down conversion in the receiver. In the FDM based approach presented here, it is convenient to spectrally separate the I and the Q channels in the RF spectrum and provide a dedicated frequency slot to each of them as shown in Figure 5 and 6. This was accomplished by adding a $2x2$ 90° RF hybrid coupler, equivalent to a Hilbert transform, for the *I* and the *Q* channels before entering the IQ mixer as shown in Figure 8. This allows the *I* and the *Q* channels to be up-converted to the lower and the upper RF sidebands independently [16].

Since both the *I* and the *Q* channels are created digitally, Hilbert transform can be straightforwardly accomplished by digital signal processing (DSP). In a practical system, this

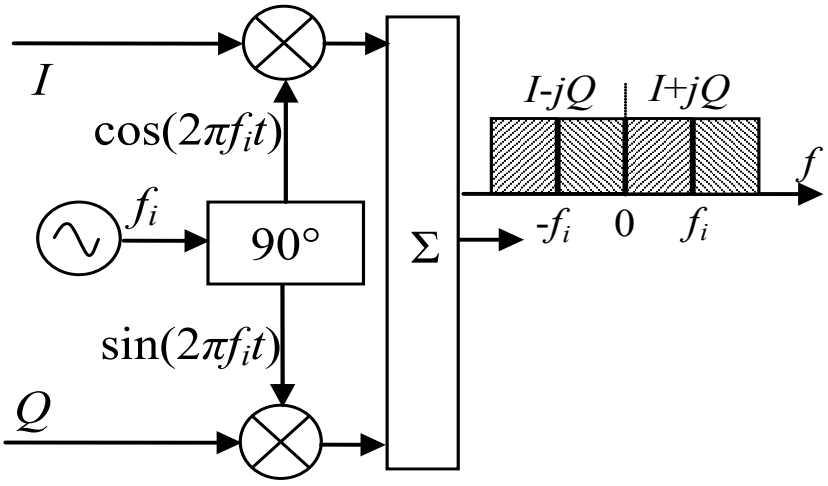

Figure 7:Schematics of IQ mixing without a 2x2 90° hybrid

allows the determination and optimization of I/Q isolation through measuring the sideband suppression ratio directly from the up-converted RF spectrum. Since the *I* and the *Q* channels are spectrally separated, if a wideband receiver is used it is also possible to use digital filters to separate them and to recover data carried by each of them. As the waveform carried by each RF subcarrier is digitally created, it can be composed of multiple digital subcarrier channels as an additional layer of frequency division multiplexing. The data rate granularity and the modulation format of tributary digital subcarriers can be flexible enough to satisfy user demand and to maximize network efficiency. In the spectra shown in Figure 5 and 6, 10 Nyquist digital subcarrier channels (100Mb/s each) are carried on each side of an RF subcarrier, where $\beta = 0$ is used as the roll-off factor of an ideal Nyquist filter [14], rendering a 100% bandwidth efficiency.

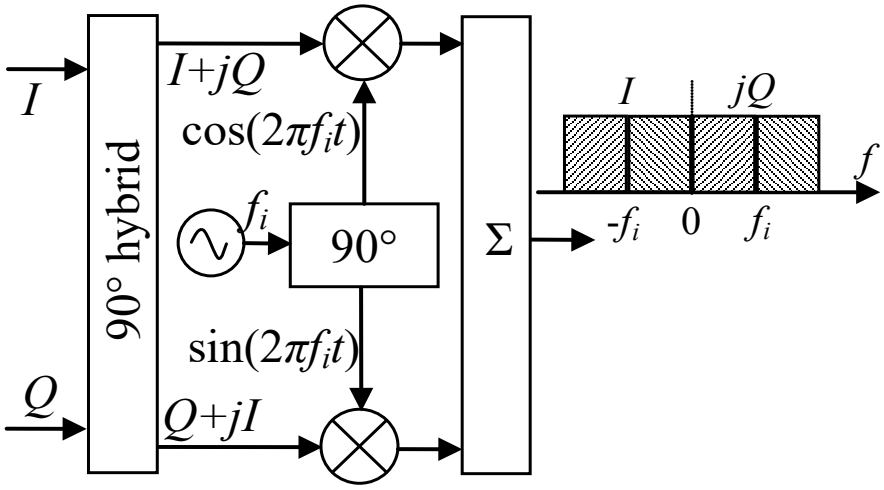

Figure 8:Schematics of IQ mixing with a 2x2 90° hybrid

For optical transmission, this composite RF signal is converted into optical domain using a dual-electrode Mach-Zender modulator and a $1x2$ 90° hybrid coupler, as shown in Figure 4, to achieve single-sideband optical modulation [9]. Figure 9 shows the SSB modulated optical spectrum measured by an optical spectrum analyzer with 0.01nm resolution bandwidth. In this experiment, a

relatively small modulation index was used to avoid signal-signal beat interference in the direct-detection receiver, so that carrier to signal power ratio is approximately 20dB.

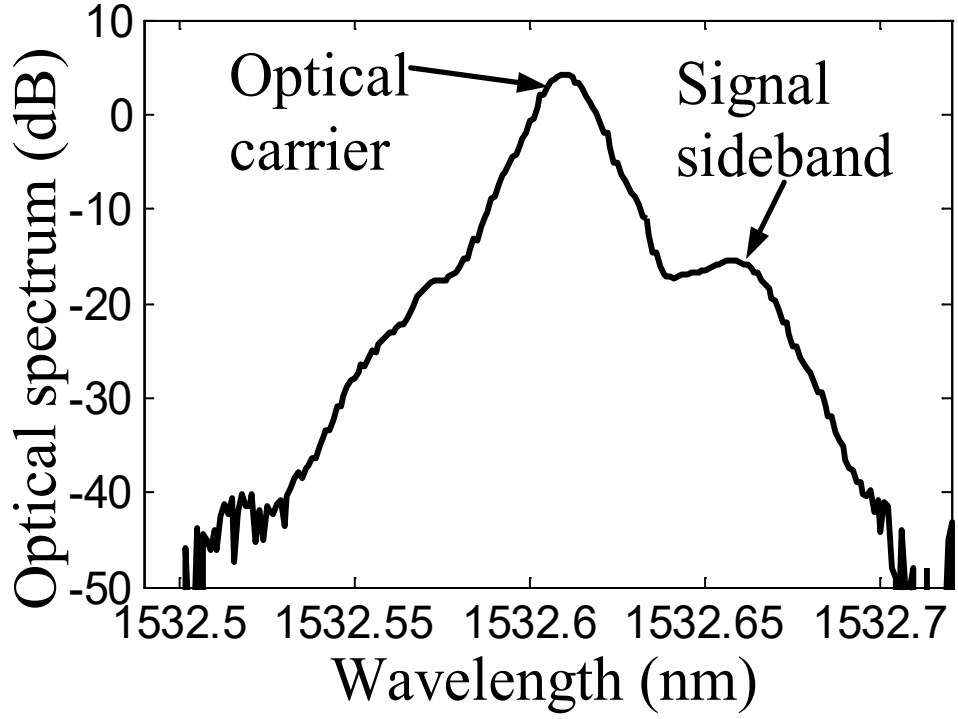

Figure 9:Single sideband optical spectrum

2.4 Detection with a high-speed receiver

If a high-speed receiver is available, all RF subcarrier channels can be digitized and processed in the digital domain to recover the data carried on each subcarrier. This includes frequency down conversion of each RF subcarrier by mixing with a digitally generated RF carrier, and phase synchronization based on the Viterbi-Viterbi algorithm [17]. Figure 10 shows an example of measured RF spectrum at the receiver after photodetection and a high-speed ADC. In this example, only two RF subcarrier channels are used at 5GHz and 7.2GHz, each carrying an *I*-channel on the lower sideband and a *Q*-channel on the upper sideband. Both the *I* and the *Q* channels are digitally created each has 1GHz bandwidth consisting 10 QPSK modulated subcarrier channels of 100Mb/s

data rate. Nyquist filters are employed to create tributary digital subcarrier channels with 100MHz bandwidth and β =10% roll-off rate. The spacing between centers of adjacent digital subcarrier channels is 110MHz, resulting in an RF bandwidth efficiency of 90%. The inset of Figure 10(a) shows spectral details around the 5GHz subcarrier revealing narrow spectral gaps between digital subcarriers.

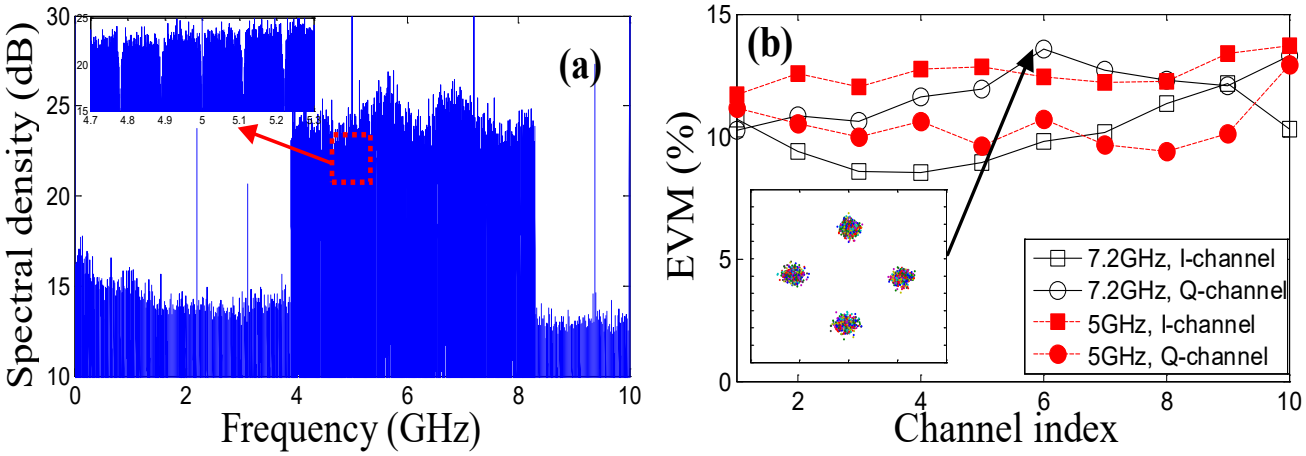

Figure 10:Two double-sideband RF subcarriers at 5GHz and 7.2GHz, each carrying I and Q channels. (a) spectrum measured with a high-speed receiver. (b) EVM of recovered digital subcarrier channels.

Because all the IQ mixers used in the experiment were built with SMA-connectorized discrete components, including splitters, hybrids, mixers and combiners, transfer function was not ideally flat across the pass-band, which is largely attributed to residual reflections from RF components and connectors. In fact, as much as 3dB transfer function ripple is observed in the spectrum across the 4GHz bandwidth as shown in Figure 10(a). This non-uniformity in the transfer function has to be minimized in practical applications by integrating all RF components onto the same circuit board. Figure 10(b) shows the error vector magnitude (EVM) [18] of all 40 recovered digital subcarrier channels. The average EVM is approximately 11%, with about 5% variation from channel to channel. As only a short fiber section is used in this back-to-back system setup, the impacts of both chromatic dispersion and optical SNR are negligible. The EVMs and their variation

across channels can be caused by the spurious reflections in the RF circuit, the crosstalk between RF subcarrier channels, and between *I* and *Q* channels of the same RF subcarrier due to the non-ideal IQ mixing.

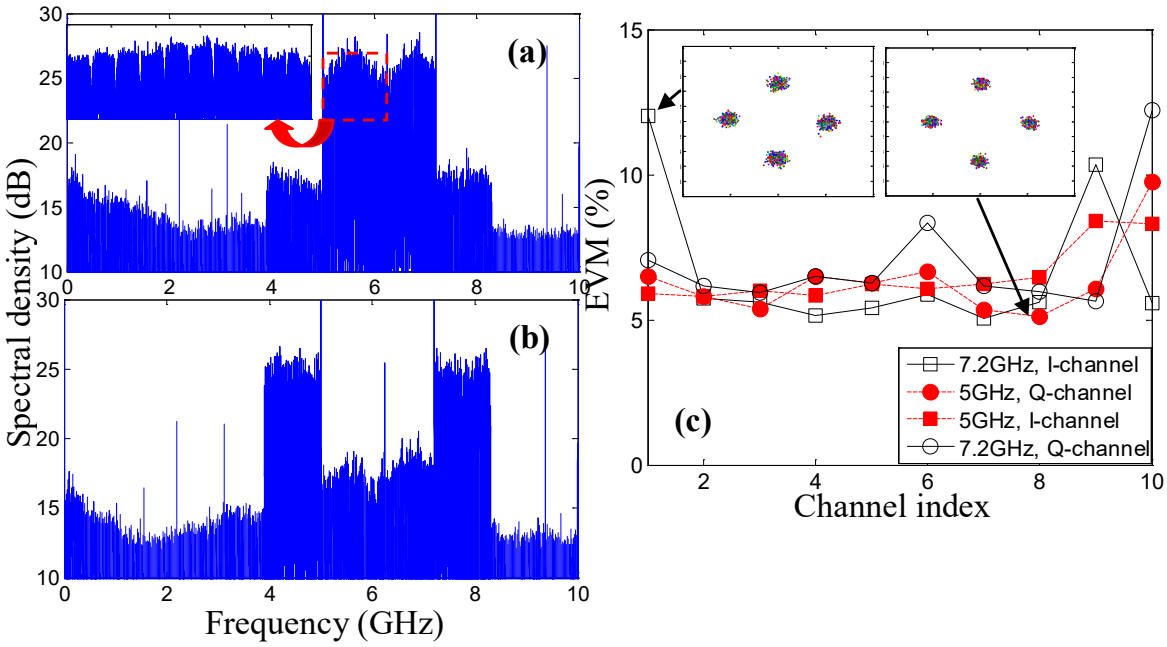

Figure 11: Two single-sideband RF subcarriers at 5GHz and 7.2GHz, each carrying an I or Q channel. (a) spectra measured with a high-speed receiver. (b) EVM of recovered digital subcarrier channels.

In order to identify the impact of various crosstalks, we used single-sideband (SSB) modulation so that the suppression of the opposite sideband can be directly measured. Figure 11(a) shows the RF spectrum in the receiver in which the *I*-channel of the 5GHz carrier and the *Q*-channel of the 7.2GHz carrier are turned-off, while in the spectrum of Figure 11(b) the *Q*-channel of the 5GHz carrier and the *I*-channel of the 7.2GHz carrier are turned-off. The opposite sideband rejection ratio is on the order of 10dB. This non-ideal sideband rejection is primarily caused by the inaccuracy of the 90° hybrid, the efficiency mismatch of the two mixers, as well as the spurious reflections and interferences caused by RF connectors used in constructing the IQ mixer. Figure 11(c) shows the values of EVM of all 20 digital subcarrier channels in each spectral setting shown in Figure 11(a)

and 11(b). The overall average EVM in the SSB modulated system is 6.6%. Although the spectrum shown in Figure 11(b) has widely separated spectral components between the two RF subcarriers, the EVM values are very similar to those measured with the spectrum shown in Figure 11(a) where spectral components of the two RF subcarriers are separated only by 10MHz. This indicates that the crosstalk between different RF subcarrier channels is negligible. In comparison to the performance of SSB modulated system, the degradation of EVM in double-sideband (DSB) system shown in Figure 10 is primarily attributed to the crosstalk between the *I* and the *Q* channels of the same RF carrier due to the non-ideal sideband rejection of the IQ mixer.

2.5 Detection with narrowband receiver

Although the investigation of system performance using a wideband receiver discussed above helps identifying sources of crosstalk, the hybrid system presented here is most suitable for narrowband receivers based on RF frequency down-conversion of subcarrier channels. Figure 12(a) shows the block diagram of RF frequency down-conversion in the receiver using an IQ mixer. A low-pass filter is placed before each ADC to prevent aliasing of high frequency components. In this experiment, 1GHz analog bandwidth is required for each ADC to accommodate the data rate carried

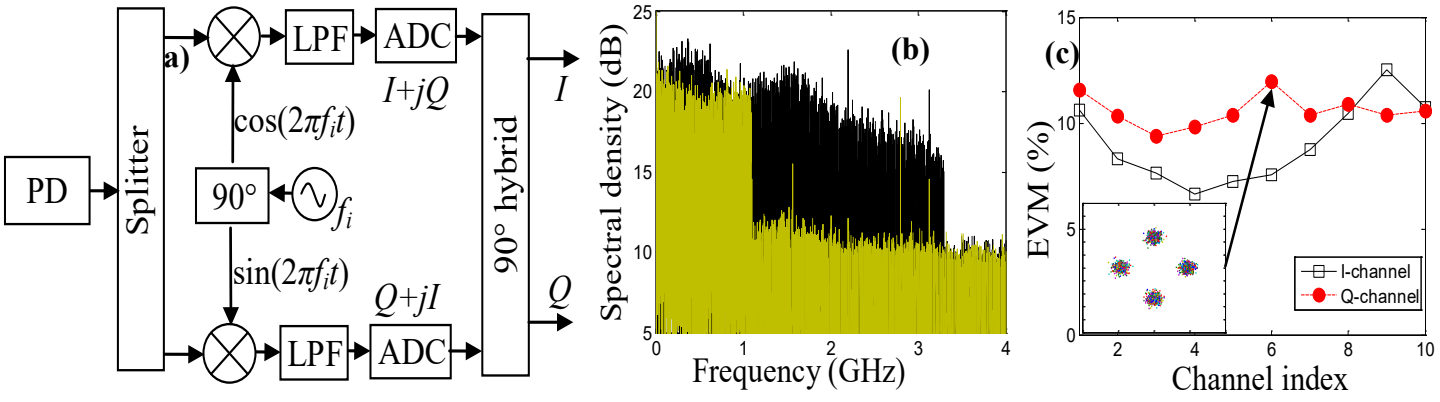

Figure 12:(a) block diagram of frequency down-conversion using based on IQ mixing in the receiver, (b) spectra of recovered I and Q channels on the 7.2GHz RF carrier, and (c) measured EVM of I and Q channels

by each RF carrier. Figure 12(b) shows the spectra of recovered *I* and *Q* channels from the 7.2GHz RF carrier. In this example, DSB modulation is used for both 5GHz and 7.2GHz subcarrier channels as shown in Figure 10(a). The EVM of the recovered constellation diagrams are shown in Figure 12(c) with an average value of approximately 10%, similar to that obtained with the wideband receiver.

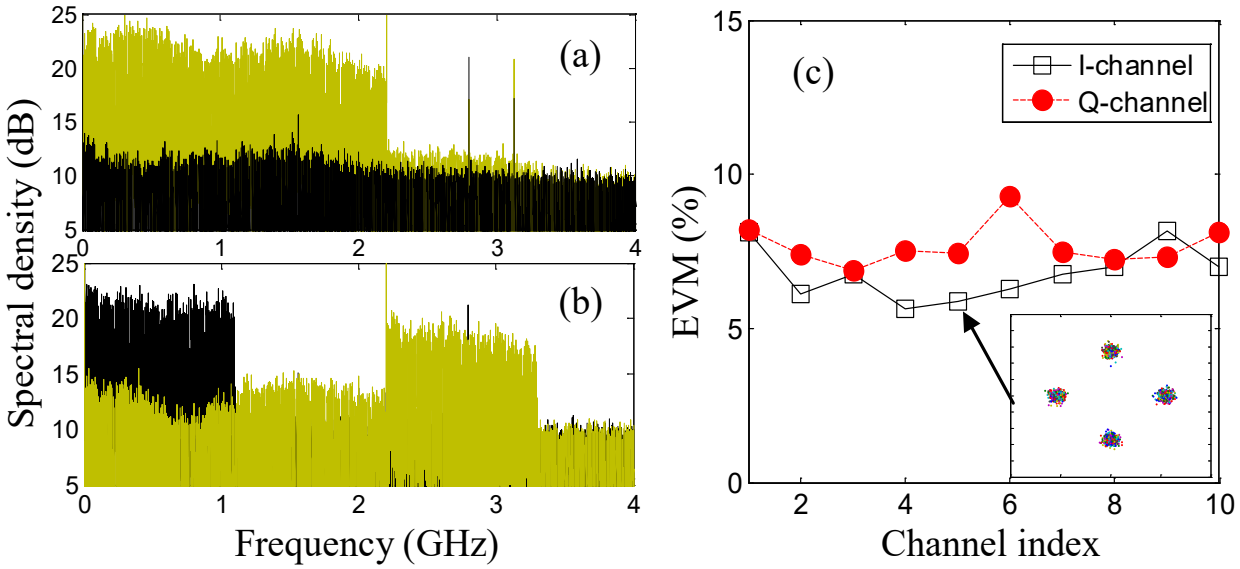

Figure 13: (a) and (b) spectra of recovered I and Q channels on the 7.2GHz RF carrier with SSB modulation, and (c) measured EVM of I and Q channels

Note that in the RF frequency down-conversion process using an IQ mixer, the phase of the RF local oscillator has to be synchronized to the RF carrier of the received signal so that the *I* and the *Q* channels can be separated.

Figure 13(a) and (b) show the spectra of recovered *I* and *Q* channels on the 7.2GHz RF carrier with SSB applied on both the 5GHz and the 7.2GHz RF carriers, corresponding to the IF spectra shown in Figure 11(a) and (b), respectively. Because the crosstalk between the *I* and the *Q* channels of the same RF subcarrier does not exist in this SSB modulated system, the average EVM is approximately 7.2%, which is comparable to that obtained with the wideband receiver

for SSB modulated signal. But the sampling rate of ADC required in this narrow band receiver is much lower, which is determined only by the width of the baseband carried on each RF subcarrier.

2.6 Conclusion

We have demonstrated a circuit-oriented approach based on digital-analog hybrid-SCM, in which multiple digitally generated subcarriers are aggregated through RF oscillators and IQ mixers for frequency up- and down- conversions. Taking advantages of the flexibility provided by digital electronics and the wide bandwidth capability of analog RF circuits, this parallel and modular approach allows the scale-up of per-wavelength data rate without increasing the bandwidth of digital electronics, such as ADC and DAC. While digital electronics are flexible enough to allow software controllable data rate granularity through advanced modulation formats, digital filtering and digital signal processing, RF electronics has the potential to provide highly efficient multiplexing and demultiplexing of subcarrier channels. We have constructed a hybrid subcarrier system with 4 RF subcarriers to provide an 8GHz aggregated RF bandwidth. Modulating waveform on each RF subcarrier channel is digitally created based on Nyquist FDM format with 1GHz bandwidth on each sideband of the subcarrier consisting of multiple low rate digital subcarriers. Using a direct-detection optical receiver, we show that RF down conversion can be accomplished either in the digital domain with a high-speed receiver, or in RF domain with low speed receivers after RF IQ down-conversion mixing. The impact of crosstalk has been investigated by comparing DSB and SSB modulated systems. Although crosstalk between adjacent RF subcarrier channels can be minimized with proper spectral confinement through Nyquist filtering, crosstalk between opposite sidebands of the same RF carrier may become a limiting factor if the IQ mixer is not ideally constructed. For practical applications, high quality IQ mixers

and RF oscillators with frequency control and phase locking can be integrated and packaged together to minimize reflection and pass-band ripples.

Chapter 3: QDB Modulation to reduce DSP resource requirement

3.1 Introduction

This chapter will discuss a correlative coding scheme to relax the resource requirements for the implementation of filters to avoid the cross talk between the two channels of a frequency division multiplexed DSCM system, while achieving 2bits/s/Hz spectral efficiency.

Spectral efficiency and bit rate per channel are important factors in any communication systems. In addition, the resources required for implementing digital signal processing (DSP) is one of the main factors for practical realization using both FPGAs and ASICs. To implement a Quadrature Phase Shift Keying-frequency division multiplexing (QPSK-FDM) transmitter and receiver on a FPGA, digital filters have to be used to shape the binary sequence before modulating into a QPSK signal. Ideally, in order to maximize the spectral efficiency while minimizing inter-channel crosstalk and inter-symbol interference, Nyquist Filters with infinitely sharp edges have to be used to cut off spectral components beyond $\pm 1/T$, where T is the bit duration. The roll-off factor of a Nyquist filter β specifies the sharpness of the edges with $\beta = 0$ for the sharpest edges. However, practical implementation of an ideal Nyquist filter with $\beta = 0$ can be extremely challenging on both FPGAs and ASICs, as it requires infinite number of taps. A digital filter with shallower edges can reduce the resources requirement, but would either introduce inter-channel crosstalk if FDM channels are tightly spaced, or would reduce spectral efficiency by reserving a spectral guard band between adjacent FDM channels.

As far as we know, the previous works [28-31] on QDB are on optical domain and not on digital domain. The only work on spectral shaping of optical quadrature duobinary has been demonstrated by [28] using coherent receiver. Other than this, many of the works [29-31] on QDB are using coherent detection. In this research, we have used electrical quadrature duobinary in a digital

subcarrier multiplexing system to estimate the reduce in DSP resources required to implement on a FPGA instead of QPSK by taking advantage of the spectral shape of QDB using direct detection.

3.2 Duobinary Coding

Duobinary coding is known for the reduced spectral bandwidth. We demonstrate that the combination of duobinary coding and digital filtering can significantly reduce the overall digital resources requirement for DSP.

To convert a binary signal into a duobinary signal, also known as a partial-response signal [20], controlled correlation should be introduced among adjacent bits. This is achieved by passing a binary signal through a one-tap delay-and-add filter [23] as shown in Figure 14.

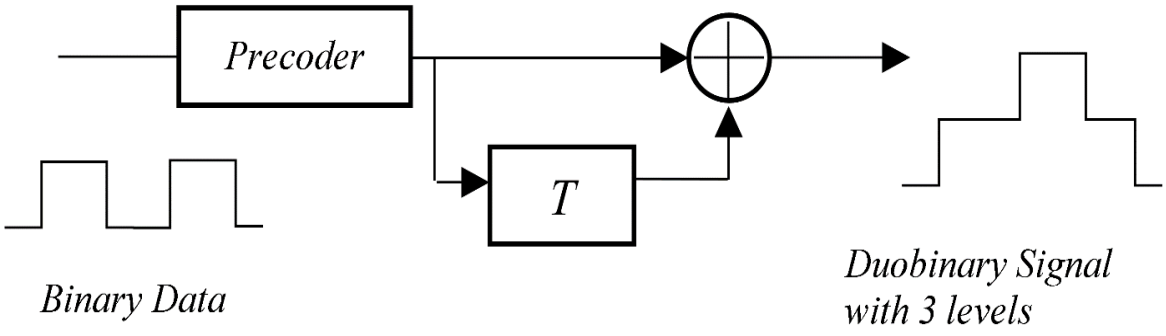

Figure 14: Duobinary signal generation using a one-tap delay and add filter

In this coding process, the original binary NRZ sequence a_k is first pre-coded into a new binary sequence b_k according to Equation (1),

$$b_k = a_k \oplus b_{k-1} \qquad (1)$$

This pre-coded binary sequence b_k is then fed to a one-tap duobinary filter, as shown in Figure 14, to generate a duobinary sequence c_k

$$c_k = b_k + b_{k-1} \qquad (2)$$

The duobinary signal can later be converted back to the original binary sequence by making individual decisions i.e. symbol-by-symbol basis using Equation (3),

$$a_k = c_k mod\ 2 \qquad (3)$$

The introduction of controlled correlation between adjacent bits leads to an important change in the spectral shape of the signal which concentrates most of the signal energy closer to the carrier. If the input binary sequence is an ideal NRZ pulse train with amplitude *A* and bit length *T*, the power spectral density (PSD) of the resulted duobinary signal is [20] [23],

$$S(f) = A^2 T sinc^2[2fT] \qquad (4)$$

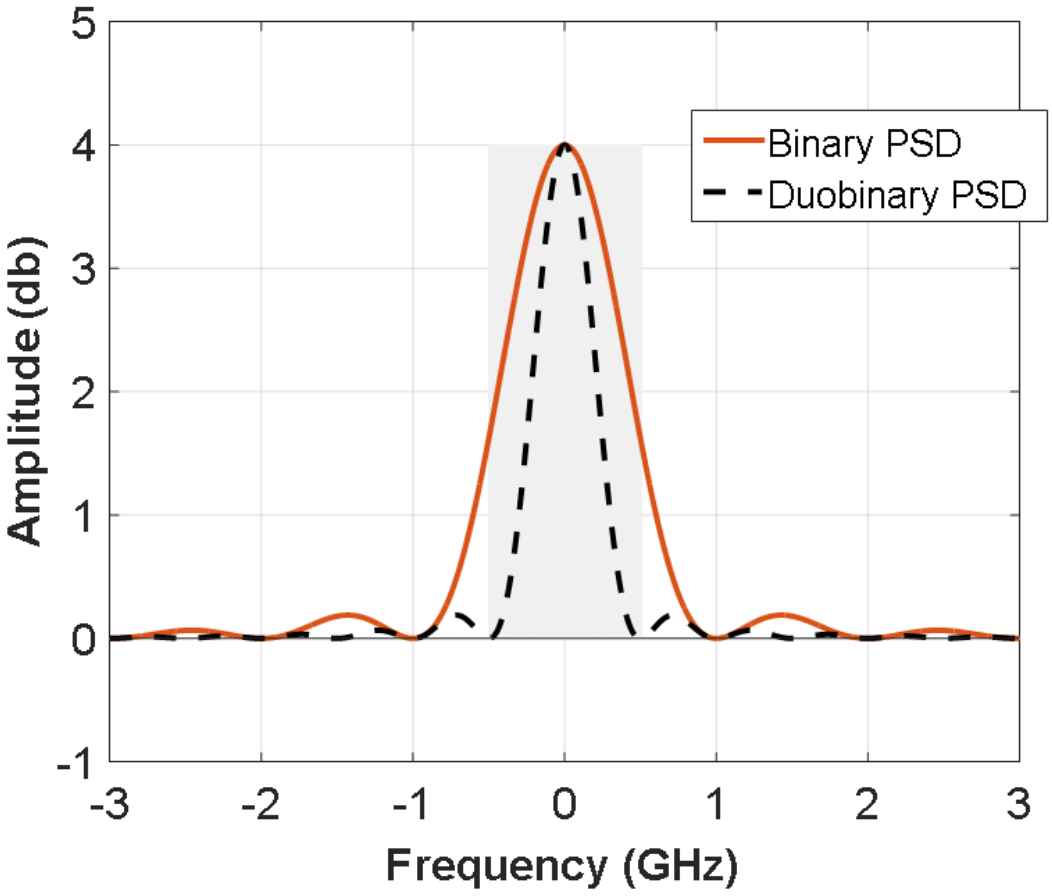

Figure 15: Spectral shaping comparison between binary and duobinary signals, most of the required spectrum for demodulation is under shaded section.

The comparison of PSD of binary and duobinary coded signals is a shown in Figure 15. It clearly shows that transforming from binary to duobinary approximately halves the 3-dB spectral width. However, according to the sampling theorem, the spectral bandwidth required to accommodate a duobinary coded signal is the same as that of a binary coded signal, although the spectrum of duobinary signal is reshaped due to the controlled inter-symbol correlation. Nevertheless, the reshaped spectrum of duobinary coding can be utilized to relax the requirement on the roll-off factor of digital filters, and thus to reduce the resources required to construct these filters.

3.3 Quadrature Duobinary Modulation

Quadrature duobinary signal is a slightly modified version of QPSK/4QAM [21]. It is a modulation scheme where duobinary signal is modulated onto the in-phase (I) and quadrature (Q) components of a carrier. Similar to QPSK generation, a single binary data stream is first partitioned into two channels through a serial-to-parallel (S/P) conversion. Each of these channels is then coded into duobinary format along with precoding as described by Equations (1) - (3). These two duobinary shaped channels are converted into I and Q phase components before added together generating the final QDB signal, as shown in the Figure 16.

The QDB signal has nine points in the constellation as shown in the Figure 16. Out of these 9 points, 4 corner constellation points represent the digital bits (1, 1), and the 4 opposite points along the x- and y-axes represent bits (1, 0) and (0, 1). Here we point out that QDB signal has the same spectral shape as duobinary as the binary-to-duobinary transformation has been applied in

the coding process. Thus, the 3dB spectral bandwidth of a QDB signal is half compared to that of a QPSK signal of the same data rate.

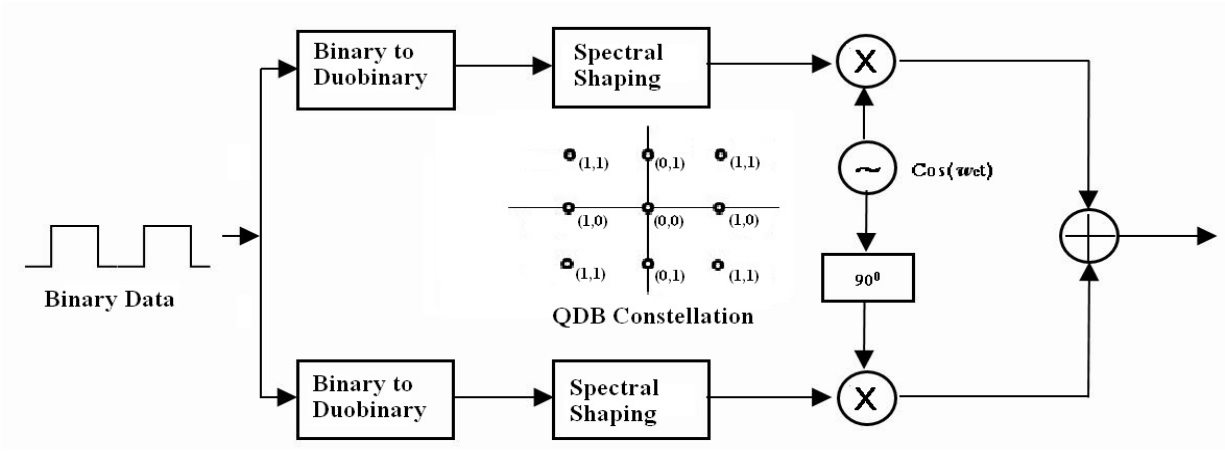

Figure 16: Block diagram to generate Quadrature Duobinary Signal.

Similar to the comparison of bandwidth requirement between binary and duobinary signals, QDB signal has a narrower 3dB bandwidth compared to QPSK, but the minimum bandwidth reserved for a QDB channel in FDM still has to be the same as that of a QPSK channel, which is $1/(2T)$.

However, an advantage of spectral shaping by transforming QPSK into QDB is the much relaxed requirement on the roll-off factor of the digital filter, and thus the reduced requirement on FPGA resources to implement the digital filter.

$$H(f) = \begin{cases} \frac{\pi f T}{\sin(\pi f T)}; & |f| \le \frac{1-\beta}{2T}; 0 \le \beta \le 1 \\ \frac{\pi f T}{\sin(\pi f T)} \cos\left\{\frac{\pi T}{2\beta}\left(|f| - \frac{1-\beta}{2T}\right)\right\}; & \frac{1-\beta}{2T} \le |f| \le \frac{1+\beta}{2T} \\ 0; & |f| \ge \frac{1+\beta}{2T} \end{cases} \quad (5)$$

The transfer function of a Nyquist filter normally used for QPSK is shown in Equation (5), where β is the roll-off factor and T is the bit duration. For a QPSK signal, the ideal Nyquist filter

should have a cut-off frequency $F_c = 1/(2T)$ with a roll off factor $\beta = 0$. This infinitely sharp filter completely cuts off all spectral components beyond $\pm F_c$, which minimizes inter-channel crosstalk with the neighboring FDM channels while without the need of a spectral guard band between them. However, implementing a Nyquist filter digitally with $\beta = 0$ is practically impossible because the need of infinite number of taps. An increase of β -value would expand the spectral width of each FDM channel to $(1 + \beta)F_c$, resulting in either a reduced spectral efficiency or an increased inter-channel crosstalk.

In comparison, a QDB signal would require a more relaxed roll-off factor requirement on the digital filter. This is because the spectral shape of QDB has most of its energy concentrated close to the carrier. We redefined the Nyquist filter transfer function as shown in Equation (6) to take advantage of the reshaped QDB spectrum,

$$H(f) = \begin{cases} \frac{\pi f(1+\beta)T}{\sin(\pi f(1+\beta)T)}; & |f| \le \frac{1-\beta}{2(1+\beta)T}; 0 \le \beta \le 1 \\ \frac{\pi f(1+\beta)T}{\sin(\pi f(1+\beta)T)} \cos\left\{\frac{\pi(1+\beta)T}{2\beta}\left(|f| - \frac{1-\beta}{2(1+\beta)T}\right)\right\}; & \frac{1-\beta}{2(1+\beta)T} \le |f| \le \frac{1}{2T} \\ 0; & |f| \ge \frac{1}{2T} \end{cases} \quad (6)$$

This modified filter transfer function cuts off all spectral components beyond $\pm 1/(2T)$, independent of the β value, while the full-width at half-maximum (FWHM) bandwidth changes with the β value. Figure 17 and 18 shows the comparison between traditional Nyquist filter defined by Equations 5 and the modified one defined by Equation 6, together with the spectra of QPSK and QDB modulated signals. Here the modified Nyquist filter defined by Equation 6 is specially designed to work with QDB modulated signal, for which the slower roll-off within the bandwidth of $\pm 1/(2T)$ has minimum impact in the signal constellation diagram as QDB has a much-concentrated spectrum near the carrier.

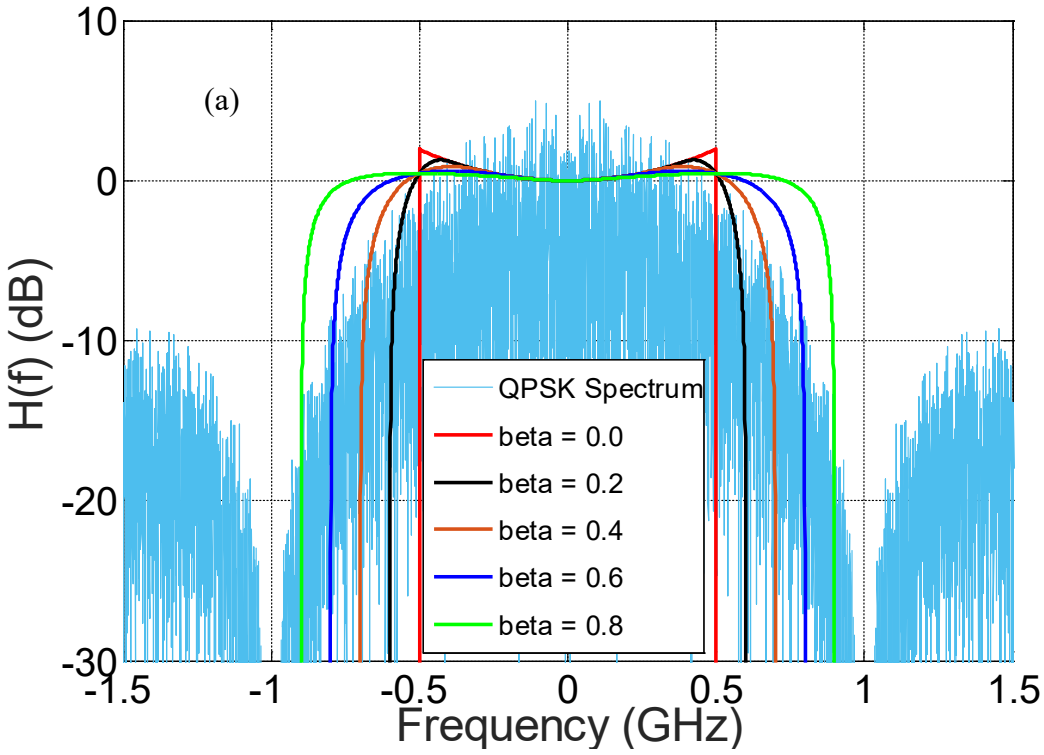

Figure 17: Transfer function of the Nyquist Filter used for QPSK spectral shaping

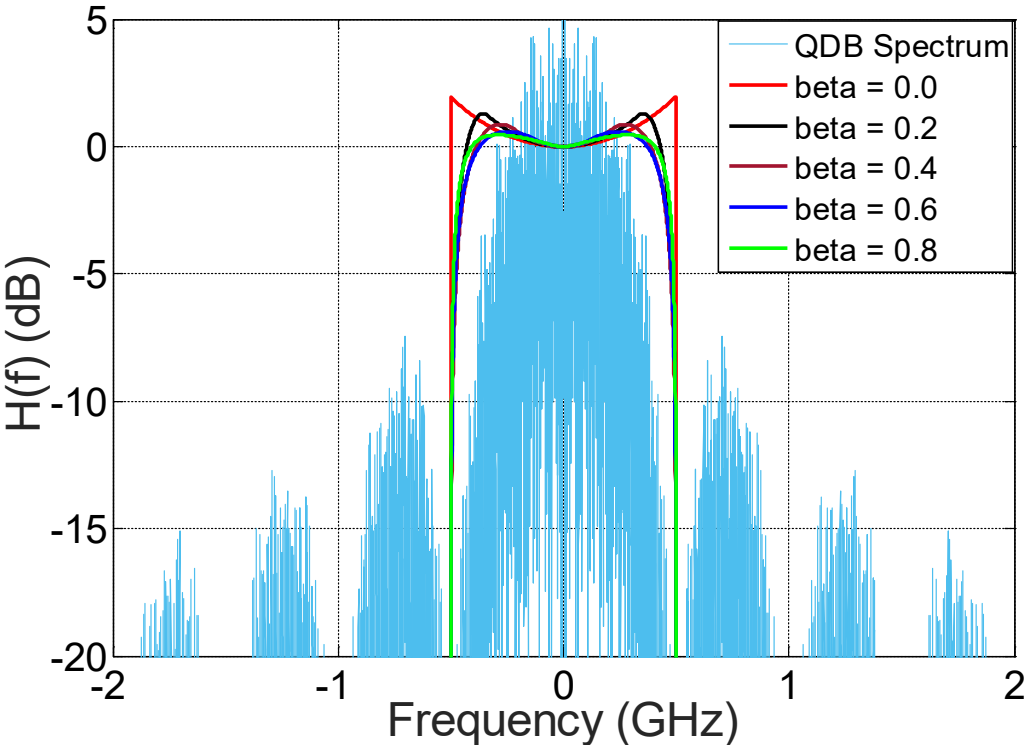

Figure 18: Transfer function of the Nyquist Filter used for QDB spectral shaping

Note that in comparison to QPSK, a drawback of QDB coding is an approximately 2dB receiver sensitivity degradation primarily due to the reduced separation between data points in the 9-point constellation diagram. Nonetheless, most of the sensitivity loss can be recovered by employing Maximum likelihood sequence estimation (MLSE) method in the receiver [24] [25]. We show that including QDB precoding, digital FIR filtering and MLSE implementation, the overall resources requirement for QDB is still significantly less than that required for QPSK to approach the theoretical limit of 2bits/s/Hz spectral efficiency in an FDM system.

3.4 OSNR requirement and resource estimation

In a QDB receiver, the relationship between the bit error rate (BER) and the signal-to-noise-ratio (SNR) can be expressed as [21] [22],

$$BER = \frac{3}{2} Q\left(\frac{\pi}{4}\sqrt{2SNR_b}\right) \qquad (7)$$

where, $Q(x)$ is the complementary error function, and SNR_b is the SNR per bit. In an optical system, if we assume the system performance is limited by the signal-ASE beat noise, SNR_b is related to the optical-SNR (OSNR) approximately by,

$$SNR_b \approx \frac{\Delta v_{0.1}}{2\Delta f} OSNR$$

where $\Delta v_{0.1}$ is the optical bandwidth of 0.1nm, and Δf is the baud-rate of the signal. For an optical signal with a single polarization, the OSNR is defined as,

$$OSNR = \frac{P_s}{2\rho_{ASE}}$$

where, P_s is the optical signal power, and ρ_{ASE} is the optical noise power within a 0.1nm bandwidth. In comparison, the BER in case of QPSK receiver is given by $= Q(\sqrt{2SNR_b})$, and

therefore the required SNR for QPSK is approximately 2dB lower than that for QDB to achieve the same BER.

The estimation of FPGA resources requirement for implementing the Nyquist filter is accomplished with System Generator program provided by Vivado 2015.4 along with Simulink. To provide a practical example, FIR Compiler 7.2 module is used to implement the digital filter on a Vortex7 FPGA XC7VX690T-1FFG1761C. This device has 3,600 DSP slices, 433,200 Look-up tables (LUT), and 866400 flip-flops (FF). For resources estimation, first we calculated the number of taps required for a given roll-off factor β. Among a number of empirical formulas available for this purpose, we estimated the number of taps, *N*, based on [26],

$$N = \frac{-20log_{10}\left(\sqrt{\delta p \times \delta s}\right) - 13}{14.6\delta f} + 1 \qquad (8)$$

where δp is the passband ripple, δs is the stopband rejection, and $\delta f = (f_{stop} - f_{cutoff})/F_s$ with f_{stop} and f_{cutoff} representing the frequencies at the beginning of the stopband and at the end of the passband. In the resource estimation, we have used the stopband rejection ratio of 40dB, the passband ripple of 0.001dB, and a sampling frequency of F_s = 25GHz.

Table I shows the breakdown of FPGA resources required to implement a Nyquist filter, including blocks needed for DSP, lookup tables, and flip-plops. Because the number of taps increases drastically with the decrease of the β value, the resources on FPGA required to implement a Nyquist filter with β = 0.9 is significantly less than that with β = 0.1.

Table I. RESOURCE ESTIMATION AND UTILIZATION

β	DSP		FF		LUTs	
	Est	***Utl%***	***Est***	***Utl %***	***Est***	***Utl %***
0.0	*NA*	*NA*	*NA*	*NA*	*NA*	*NA*
0.1	438	12.17	27051	3.12	73735	17.02
0.5	240	6.67	5305	0.61	5049	1.17
0.9	85	2.36	5182	0.6	4850	1.12

(LUT: Look up tables, FF: Flip Flops. Est: Estimation, Utl: Utilization)

3.5 Experimental Configuration

To verify the impact of digital filter roll-off factors on the performances of QDB and QPSK coded optical systems, we have conducted experiments based on digital subcarrier multiplexing (DSCM) [27], in which digitally created QPSK and QDB channels are used as subcarriers for frequency division multiplexing. Digital processing allows the flexibility of precisely controllable spectral shape of each DSCM channel, and to achieve high spectral efficiency.

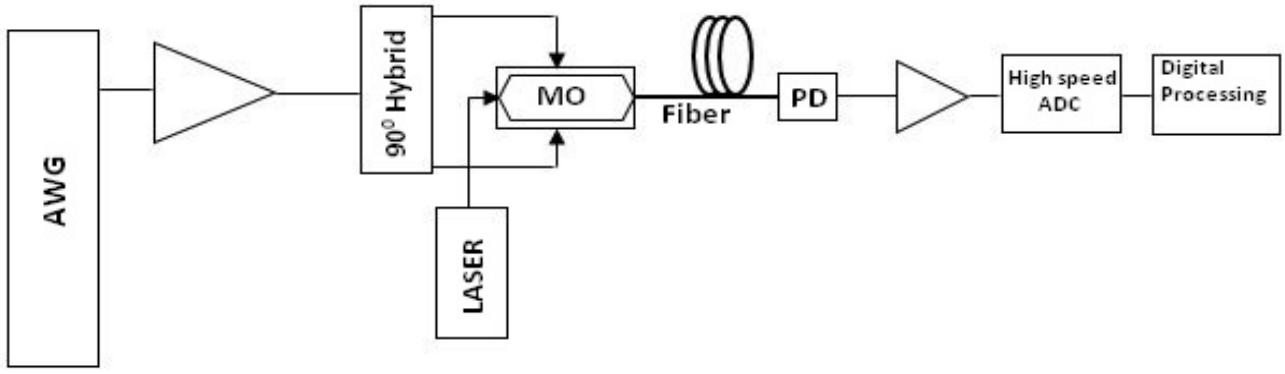

Figure 19:Experimental setup to transmit and receive QDB and QPSK signals (AWG: Arbitrary waveform generator)

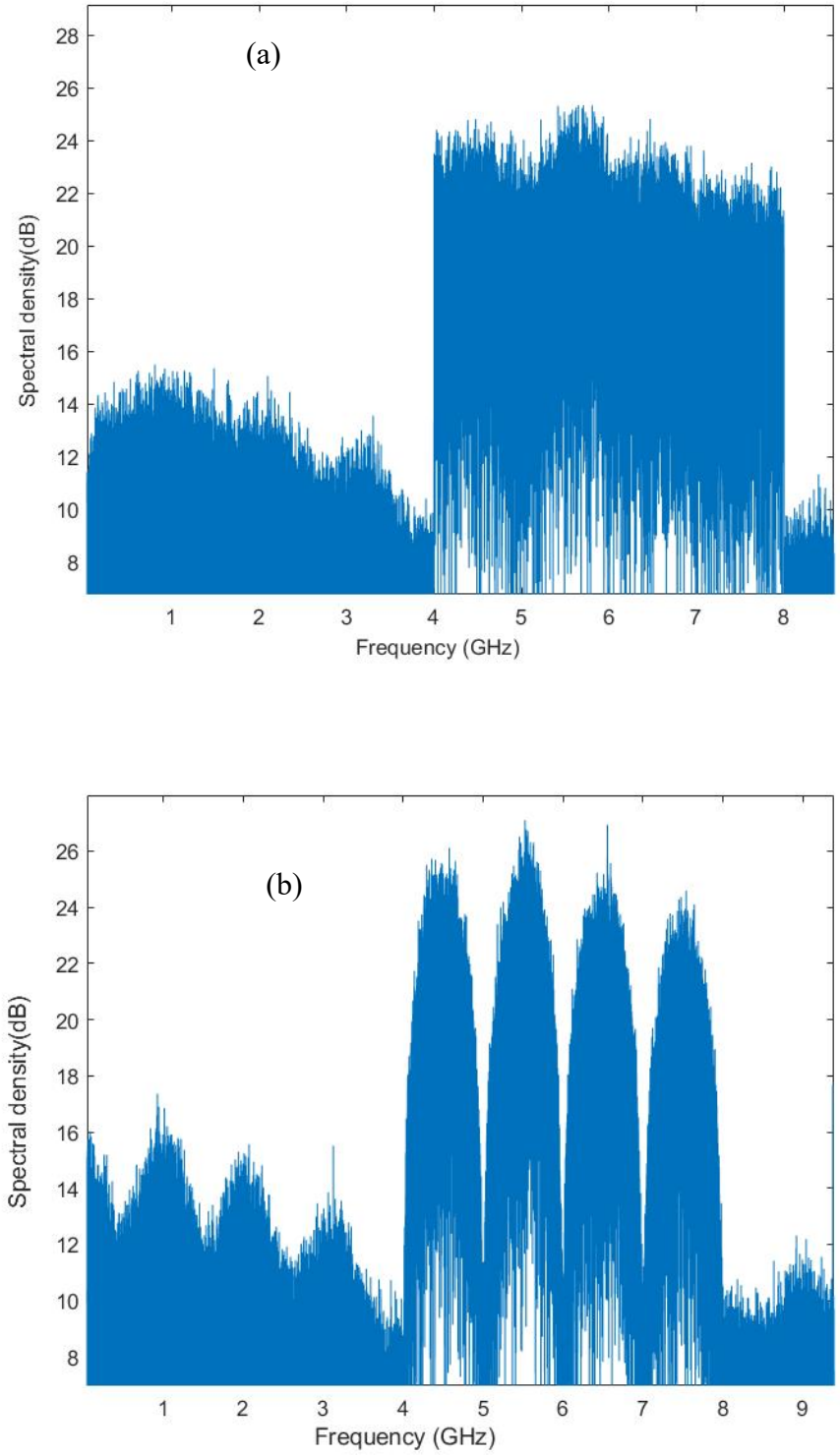

Figure 20: Received spectrum of QPSK(a) and QDB(b)

The experimental setup is shown in Figure 19, in which the signal generated by an arbitrary waveform generator (AWG) is converted into optical domain through a dual-electrode Mach-Zehnder electro-optic modulator and an RF 1×2 90^0 hybrid coupler. By properly adjusting the DC biasing point, the dual-electrode modulator allows the generation of optical signal-sideband (OSSB). The modulated optical signal is sent through an optical fiber, and detected by a high-speed photodetector with direct-detection.

The electrical signal received by the photodiode is digitized by an analog-to-digital converter (ADC) with 50GS/s sampling rate and processed in digital domain to recover the data carried by the I and the Q channels from each subcarrier. Both the QPSK and the QDB modulated signals have 4GHz analog bandwidth, consisting of 4 DSCM channels each having 1GHz bandwidth as shown in Figure 20a and 20b respectively. Thus, the total data rate is 8Gb/s for both QPSK and QDB. Various β-values for the digital filters are used to form DSCM channels in the experiment created by programing the arbitrary waveform generator using Matlab.

3.6 Simulation and Experimental Results

We first performed numerical simulations on the performance of both QPSK and QDB using Matlab to evaluate the effect of change in β values of Nyquist filters. The calculated error vector magnitudes (EVM) of constellation points are shown in Figures. 21 through 25. Figure 21 shows that increasing β from 0.0 to 0.9 leads to significant increase in the EVM for demodulated QPSK signals. This simulation was performed in the back-to-back system without considering the optical noise. The EVM degradation observed is mainly caused by the increased crosstalk between adjacent DSCM channels due to the increased spectral bandwidth and the spectral overlap when Equation 5 is used as digital filter. While using Equation 6 as filter transfer function, EVM

degradation caused by increasing β value is due to inter-symbol interference. Whereas for QDB signals, in the same region of β-values, the EVM remains almost constant and largely independent of the roll-off factor of the Nyquist filter as shown in Figure 21.

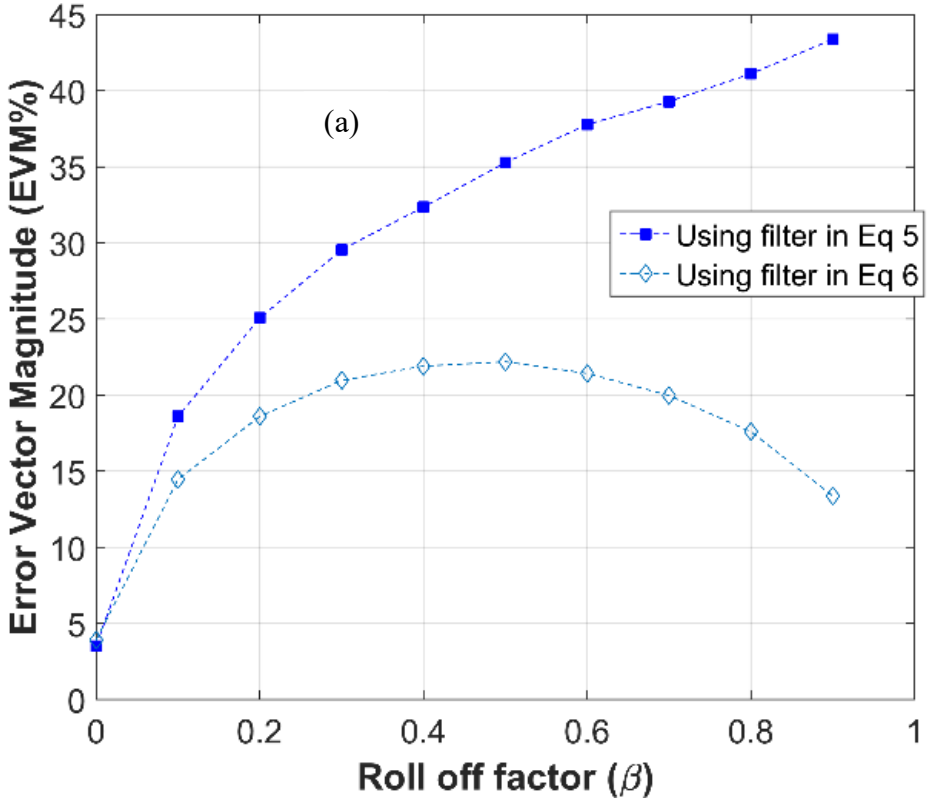

Figure 21: EVM vs beta for QPSK-FDM

In this case, the spectrum of each subcarrier channel is limited within $\pm 1/(2T)$ as indicated in Equation 6, so that no inter-channel interference is introduced by increasing β. This clearly indicates that a Nyquist filter with a much larger β-value can be used for QDB coded system without degrading both the signal quality and the spectral efficiency. Figure 23-25 shows the simulated EVM as the function of SNR_b for different values of filter roll-off factor for QPSK (Figure 23, 24) and QDB (Figure 25), respectively. Again, the EVM is very sensitive to the filter

roll-off factor β for QPSK, while there is negligible performance impact by β for QDB in the entire region of $0 < \beta < 0.9$.

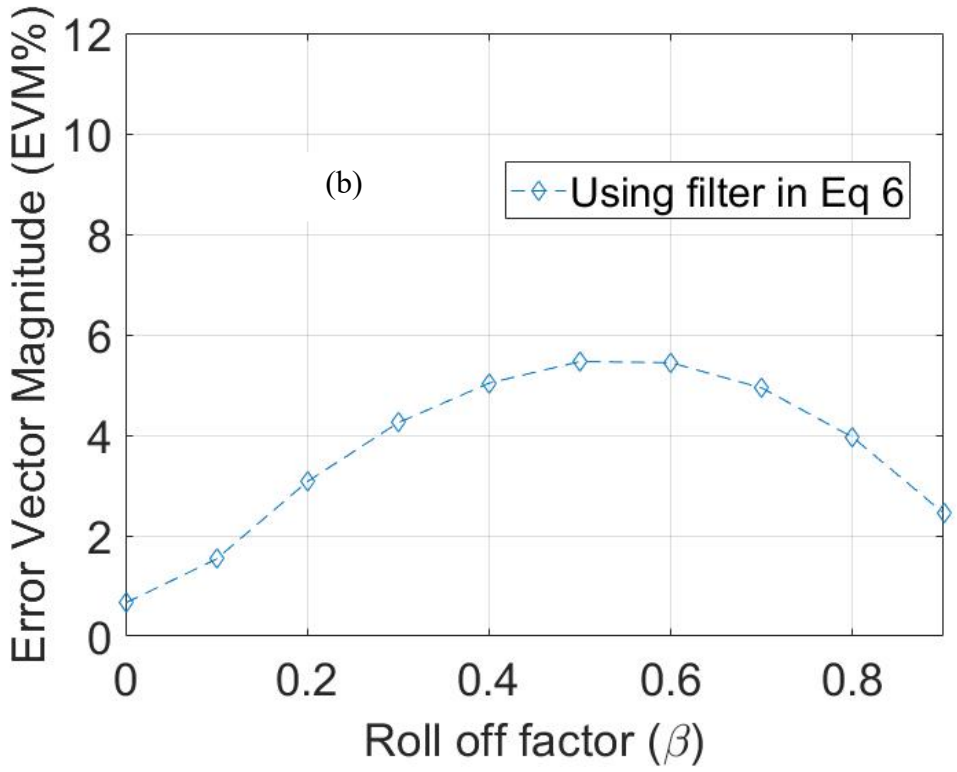

Figure 22: EVM vs beta for QDB-FDM

We then performed experiments to verify the performances of both QDB and QPSK with the experimental setup discussed in section IV. Figure 26 and 27 shows the measured EVM as the function of Nyquist filter roll-off factor β for QPSK and QDB coded signals. These experiments were performed in the back-to-back configuration so that the impact of OSNR was not included. Instead, these experiments were focused on the waveform distortion due to inter-channel crosstalk and inter-symbol interference impacted by the roll-off factor of digital filters. The experimental results shown in Figures 26-27 are consistent with the simulation, indicating that a Nyquist filter with a larger β-value can be used with QDB coded signal without degrading the EVM and the spectral efficiency.

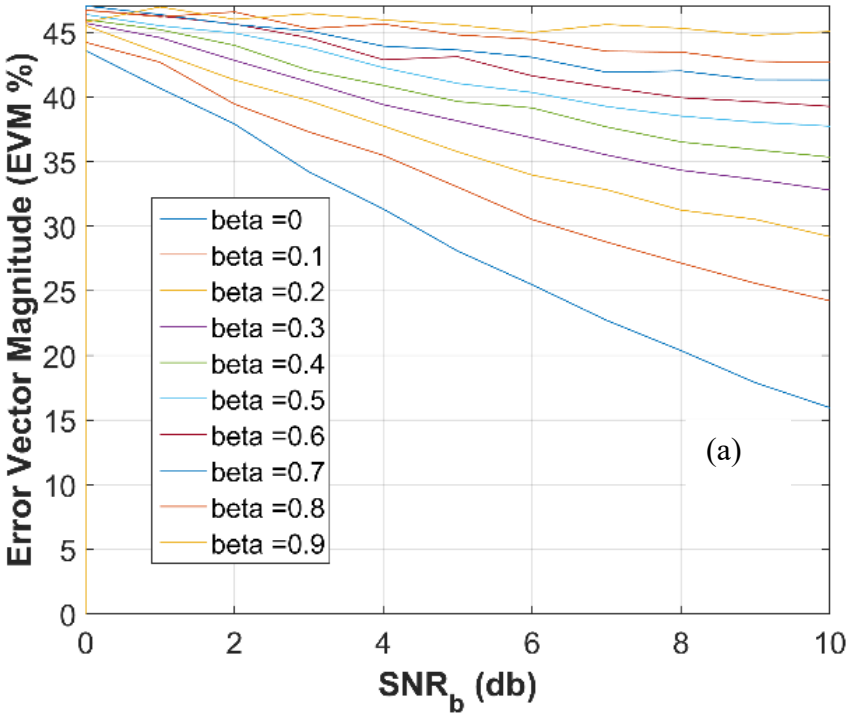

Figure 23: EVM vs SNR for QPSK-FDM using Equation 5

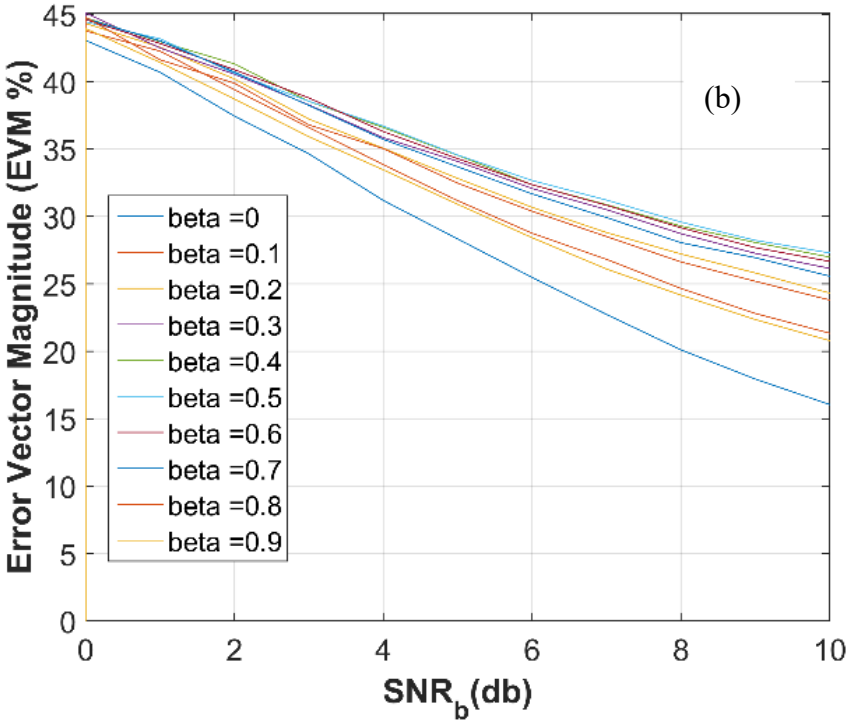

Figure 24: EVM vs SNR for QPSK-FDM using equation 6

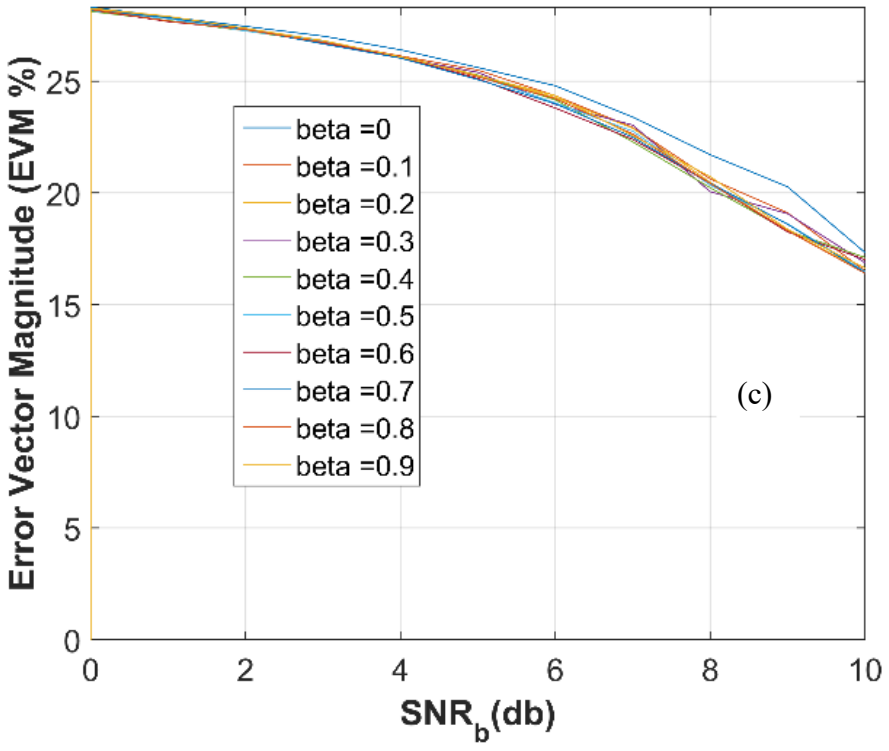

Figure 25: EVM vs SNR for QDB-FDM using equation 6

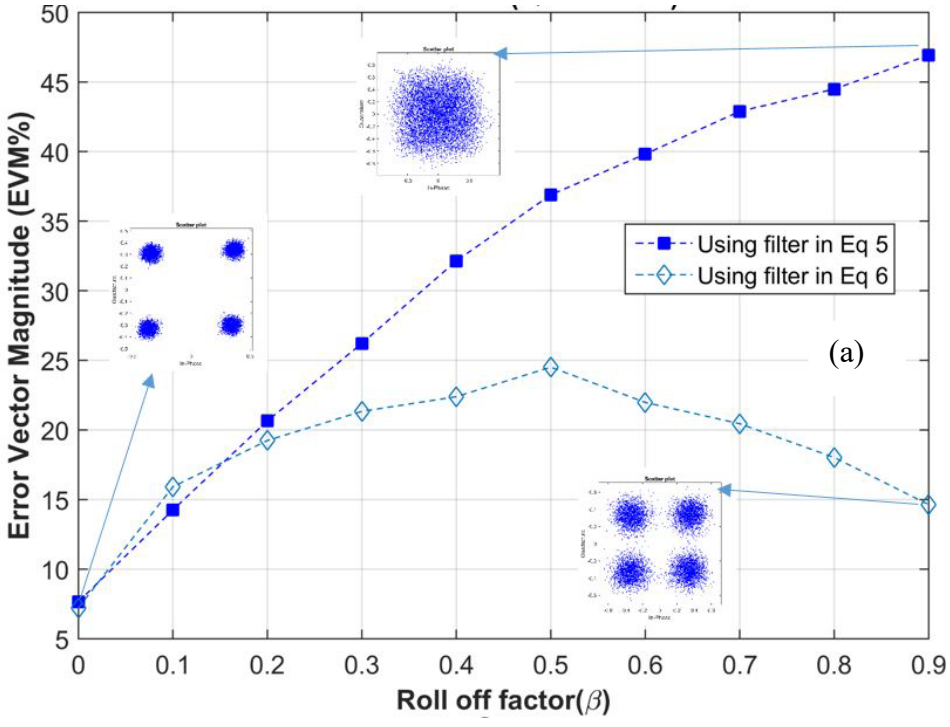

Figure 26: Experimental EVM vs beta for QPSK-FDM

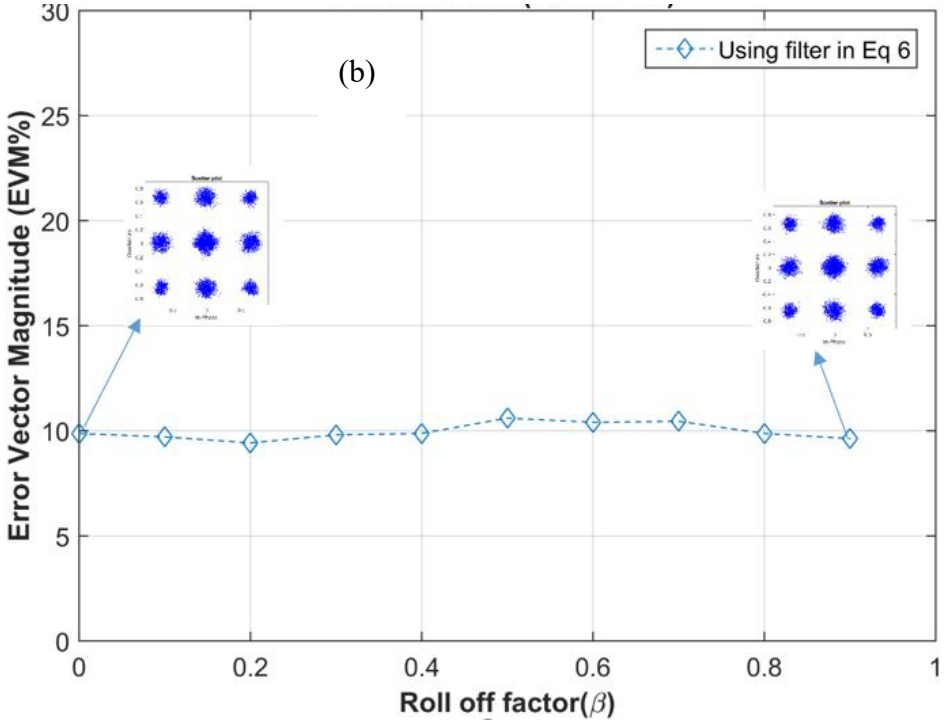

Figure 27:Experimental EVM vs beta for QDB-FDM

3.7 Sensitivity recovery possible using MLSE

QDB coding can utilize a Nyquist filter with a relatively large β-value so that significant FPGA resources can be saved in the implementation. However, there is an approximately 2dB SNR penalty in the receiver of QDB in comparison to QPSK. In fact, the symbol-by-symbol (SbS) detection scheme usually used for QPSK demodulation is sub-optimal for partial response signals such as QDB. It has been demonstrated that QDB coded signal can be demodulated with an MLSE scheme, which is able to reduce the SNR penalty from 2dB to about 0.5dB [22] [24]. The MLSE detector used for each *I* and *Q* branch of QDB coded signal has a memory length of one symbol and two states, and the trellis diagram needed to implement an MLSE detector is shown in Figure 28. We have used Viterbi algorithm [22] to implement the MLSE detector in simulation using

Matlab, and Xilinx System Generator to estimate the digital resources needed for MLSE detector, and the results are shown in Table II. It is worthwhile to notice that the extra resources needed to implement MLSE detector is only a small fraction of that required for the digital filter. Note that the 1-bit delay-and-add in duobinary pre-coding of *I* and *Q* channels before QDB signal generation also requires negligible digital resources compared to the implementation of digital filter. Thus, the overall digital resources required for QDB, including pre-coding, digital filtering and MLSE detecting, are still significantly less than those required for QPSK.

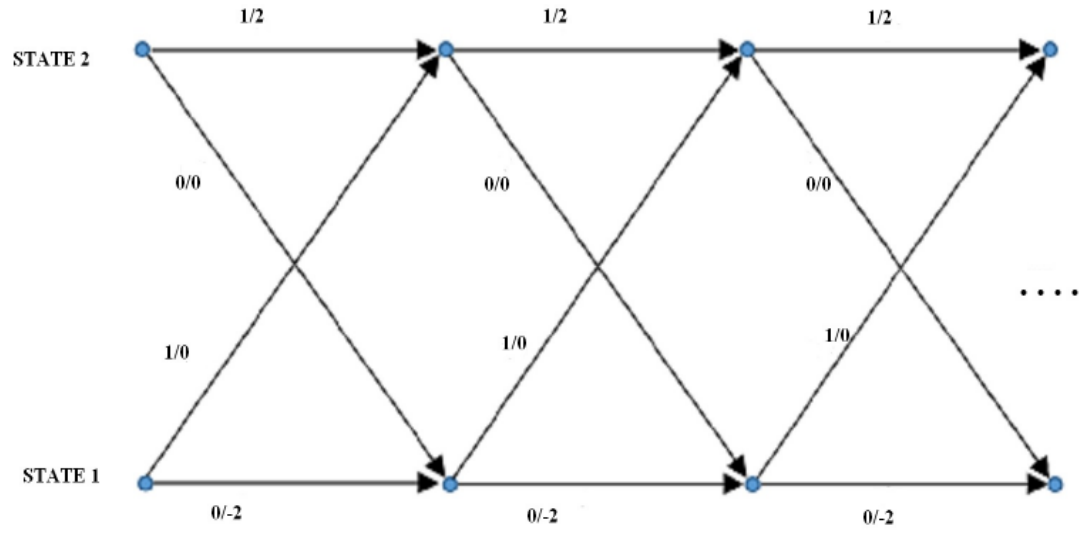

Figure 28: Trellis for MLSE detection for QDB

Table II. ADDITIONAL RESOURCES NEEDED FOR MLSE

DSP		**FF**		**LUTs**	
Est	**Utl %**	**Est**	**Utl**	**Est**	**Utl %**
8	0.22	40	0.01	230	0.05

(LUT: Look up tables, FF: Flip Flops. Est: Estimation, Utl: Utilization)

3.8 Conclusion

We have developed and demonstrated an approach to achieve 2bits/s/Hz spectral efficiency in digital subcarrier multiplexed system with significantly reduced FPGA resources for spectral shaping. The concept has been demonstrated both through numerical simulations and experiments. Actual FPGA resources requirement has been evaluated by using a Xilinx System Generator provided by Vivado design software and Simulink. This resource saving was made possible by taking advantage of the reduced spectral width of QDB signal, so that the roll-off factor of digital filter can be much relaxed without introducing inter-channel crosstalk and inter-symbol interference. The well-known 2dB SNR penalty of QDB can be mostly recovered using MLSE demodulation algorithm. Including FPGA resources required for both QDB precoding and MLSE detecting, we showed that the overall resources required for QDB is still much less than those required for QPSK.

Chapter 4: Digital pre-compensation of SOA nonlinearities in field modulated direct-detection systems

4.1 Introduction

In this chapter, a method to digitally compensate both nonlinearities introduced by semiconductor optical amplifiers (SOA) and fiber-induced chromatic dispersion is experimentally demonstrated in a field-modulated direct detection fiber-optic system. We show that digital pre-compensation is most appropriate to deal with SOA nonlinearities, and digital post-compensation in the Kramers-Kronig receiver is most effective for mitigating the impacts of chromatic dispersion and signal-signal beat interference (SSBI).

Semiconductor optical amplifiers (SOA) are very attractive for fiber-optic system applications. As a miniature-size integrable device, SOA is a good low-cost solution in optical transmitters for applications in metro optical networks [51], [52]. SOAs can be used to compensate the loss introduced by in-phase/quadrature (IQ) modulator in the transmitter for complex optical field modulation. SOAs also support wavelengths outside traditional EDFA operation windows. While fast and nonlinear responses of SOA are often used for all-optical packet switching and regeneration, relatively high nonlinearity and short carrier lifetime are disadvantages of SOAs for applications as post- and in-line optical amplifiers. Fast gain saturation of an SOA at high signal power levels leads to pattern-dependent signal waveform distortion and system transmission performance impairments [53] through self-gain modulation, self-phase modulation, inter-channel crosstalk in case of wavelength-division multiplexing.

Direct detection (DD) in an optical transmission system provides a low-cost solution compared to coherent-detection. In intensity modulation direct detection (IM/DD) systems, the impairments

induced by SOA gain saturation can be minimized through digital post-compensation [54] at the receiver. This is achieved using the digital backpropagation method by means of a nonlinear model of SOA gain characteristics. However, in case of field modulated DD systems in the presence of fiber chromatic dispersion, the post-compensation method for SOA-induced impairments will be compromised. This is because in field modulated system with DD, self-mixing of the signal optical field due to square-law detection of the photodiode leads to signal-signal beat interference (SSBI) which prevents field reconstruction in the digital domain. Additionally, in the presence of fiber chromatic dispersion, the dispersion and SOA nonlinearity induced signal distortions will be inter-coupled further complicating the field reconstruction process [54]. One way to compensate for SSBI is to provide a guard band between the carrier and the signal to isolate the effect of SSBI from the received signal. However, this leads to a loss of bandwidth efficiency by 50%. Also, digital compensation of chromatic dispersion cannot be made in a traditional DD receiver because of the spectral folding due to the square-law detection.

It has been shown in [55], [56], both SSBI compensation and dispersion compensation (DC) can be achieved by using a Kramers-Kronig (KK) receiver scheme, and hence improving the bandwidth efficiency. This is less complex and more cost effective compared to using dispersion compensating fiber or using coherent detection. In a linear system, digital DC can be performed either at the transmitter or at the receiver. But for a DD system with SSBI, digital DC has to be applied after SSBI suppression [55]. Hence using KK receiver is a good option for direct detection which allows for mitigating SSBI and compensating the impact of dispersion at the receiver. However, when a SOA is introduced into the system, the SOA induced nonlinearity will be coupled with the effect of fiber dispersion, and the linear system condition is violated. This makes both digital SSBI mitigation and DC inaccurate after the KK detection.

To solve the problem mentioned above, in this chapter we demonstrate a digital pre-compensation technique for impairments introduced by SOA gain saturation, while SSBI mitigation and dispersion compensation are performed at the KK receiver. This compensating scheme is optimum for complex field modulated optical system with KK direct detection, and allowing nonlinear components in the system such as SOA. To our best knowledge, the pre-compensation approach to mitigate SOA nonlinearities in a field modulated DD system with KK receiver has not been previously investigated.

4.2 Kramers-Kronig Receiver

The KK direct detection receiver scheme [6] allows the reconstruction of the signal complex optical field at receiver, as long as the signal has a single sideband (SSB) and satisfies the minimum phase condition. In such a case, the optical phase information of the signal can be extracted from the directly detected photocurrent. The implementation of KK scheme is as shown in Figure 29. When this optical signal is directly detected by a photodiode, a photocurrent $I(t)$ is produced. Let $E_s(t)$ be the complex envelope of the receiving band-limited signal with a

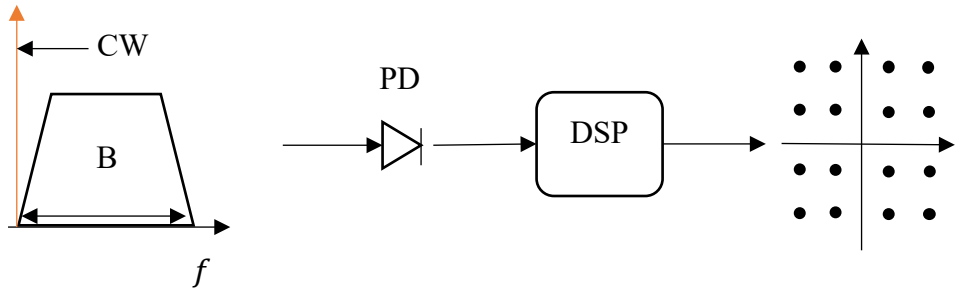

Figure 29: KK direct detection: CW is added at the left of the signal spectrum with bandwidth B

bandwidth of B. E_0 be the amplitude of continuous wave which is used as RF carrier for the signal. If I is the photocurrent produced by the photodiode, then we can reconstruct the signal $E_s(t)$ as follows [56],

$$E_s(t) = \left\{\sqrt{I(t)}\exp[i\emptyset_E(t)] - E_0\right\}\exp(i\pi Bt), \quad (1)$$

$$\emptyset_E(t) = H\{\log[I(t)]\} \quad (2)$$

where, $H\{\cdot\}$ is the Hilbert transform function, $\emptyset_E(t)$ is phase restored using KK algorithm.

Although the receiver performs square-law detection which is nonlinear, as long as the minimum phase condition is satisfied, the mixing between the carrier and the signal sideband remains linear, which allows linear reconstruction of the complex optical field [56]. The additive noise also remains additive after field reconstruction. This linear detection characteristic permits both SSBI minimization and dispersion compensation in the electronic domain at the receiver. This is under the assumption that the transmission system before the receiver is also linear.

4.3 SOA impairments and compensation

When a SOA is introduced into the system as a post amplifier in the transmitter, its nonlinear response to the optical signal is typically pattern dependent. This violates the linear system requirement for complex field reconstruction after KK detection, which would result in the reduced accuracy of SSBI mitigation and chromatic dispersion compensation. The impact of SOA nonlinearity cannot be compensated at the receiver because the simultaneous presence of both chromatic dispersion and SSBI. Since the SOA is used as the post amplifier at the transmitter and its transfer function is deterministic, it is most convenient to pre-compensate SOA nonlinear transfer function, both amplitude and phase, in the transmitter. By doing this, both SSBI mitigation and dispersion compensation can still be performed digitally at the KK receiver.

To compensate the impact of SOA nonlinearities, we first need to model the SOA nonlinear transfer function using a differential equation [54],

$$\left(1+\tau_c\frac{d}{dt}\right)h(t)=h_0-\frac{P_{in}(t)}{P_{sat}}\exp(h(t)-1) \quad (3)$$

where, $h(t)=\int_0^L g(z,t)dz$ is the integrated instantaneous gain over the SOA length L, $h_0=-lnG_0$, where G_0 is the small signal gain of the SOA. $P_{sat}=E_{sat}/\tau_c$ is the saturation power, where E_{sat} is the saturation energy of the SOA and τ_c is the effective carrier lifetime. P_{in}, is the input power to the SOA. The output optical field from the SOA is,

$$E_{out}(t)=E_{in}(t)*\exp((1-i\alpha_H)h(t)/2) \quad (4)$$

where, α_H is the chirp factor. Digital compensation of SOA nonlinear transfer function can be implemented by numerically solving the equation (3) using fourth-order Runge-Kutta method [54]. The SOA parameters in (3) such as, P_{sat}, τ_c and G_0, are deterministic. Their values can be determined experimentally by varying input power to SOA and observing output power as shown in Figure 30. At a bias current of 140mA, the carrier lifetime is approximately 350ps. This is

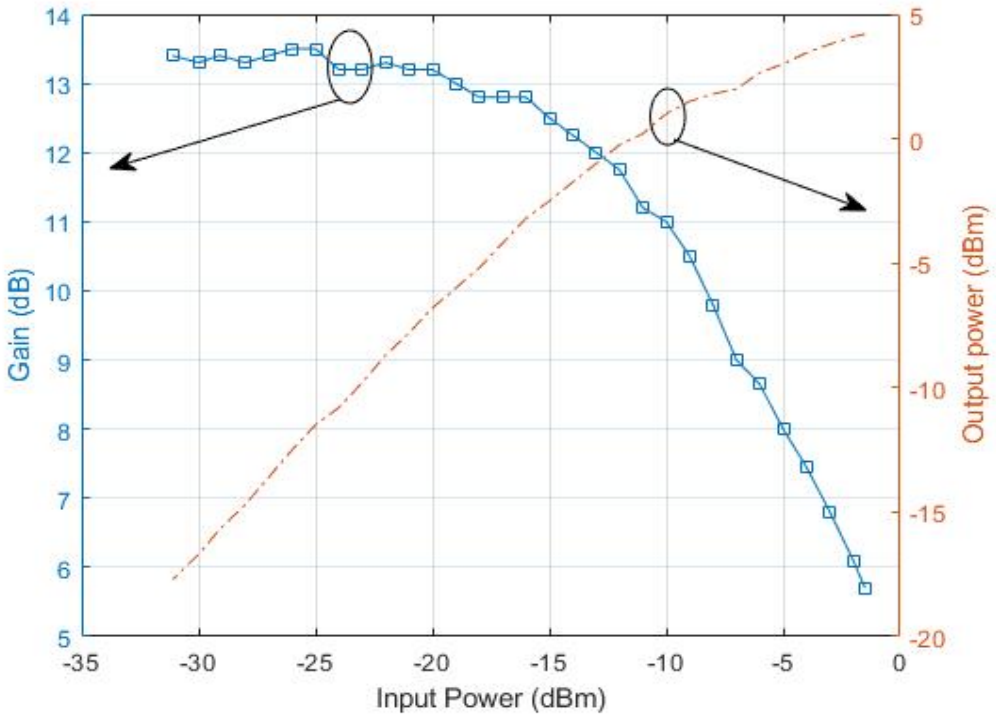

Figure 30: Experimental SOA gain characteristics

extracted from previously measured SOA carrier lifetime vs bias current data [58]. At an input power around -9dBm we see a gain suppression of 3dB in comparison to the small signal gain.

4.4 Experimental Setup

In order to demonstrate the digital pre-compensation technique of SOA nonlinearities in a field modulated DD system, we have conducted experiments using 14G baud QAM-16 modulated optical signal in an experimental setup shown in Figure 31. Carrier suppressed optical single sideband (OSSB) signal generated by an I/Q modulator is fed to a SOA after a variable optical attenuator (VOA) which adjusts the signal power. The output of SOA is combined with an optical carrier from a second external cavity laser (ECL) to satisfy the minimum phase condition for KK detection. The power of the inserted optical carrier is also controlled by a VOA to adjust the carrier to signal power ratio (CSPR). CSPR is the ratio between the optical carrier and the total signal power. Also, a polarization controller is used to align the states of polarization of the carrier component with the modulated signal sideband from the SOA before they combine. Figure 32 shows the OSSB spectrum measured by an optical spectrum analyzer with 0.01nm resolution bandwidth.

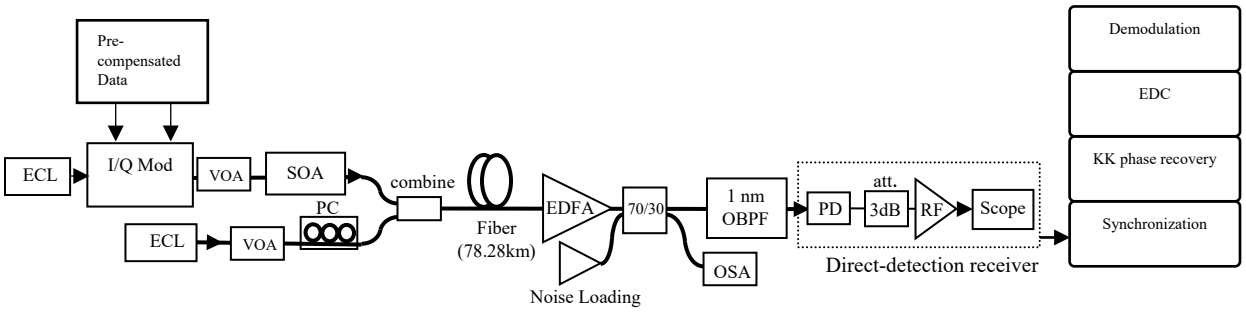

Figure 31: Experimental set up. Wavelogic Ai has the ability of selecting the output optical power, and to adjust the saturation level of the SOA or external variable optical attenuator can be used.

The combined OSSB optical signal is sent into $78.28km$ optical fiber with an effective core area of $145\mu m^2$ and $1683.02\ ps/nm$ accumulated chromatic dispersion. Another EDFA is used as an adjustable ASE noise source which is combined with the amplified optical signal through a 2×2 optical fiber coupler. This purpose of adjustable noise loading is to be able to change the OSNR at the receiver, which allows the measurement of bit error rate (BER) as the function of optical signal to noise ratio (OSNR) for system performance evaluation. A $1nm$ bandwidth optical filter is used to cut out the wide band ASE noise before the photodiode. The signal optical power that reaches at the photodiode is maintained at 5dBm throughout the experiment for consistency.

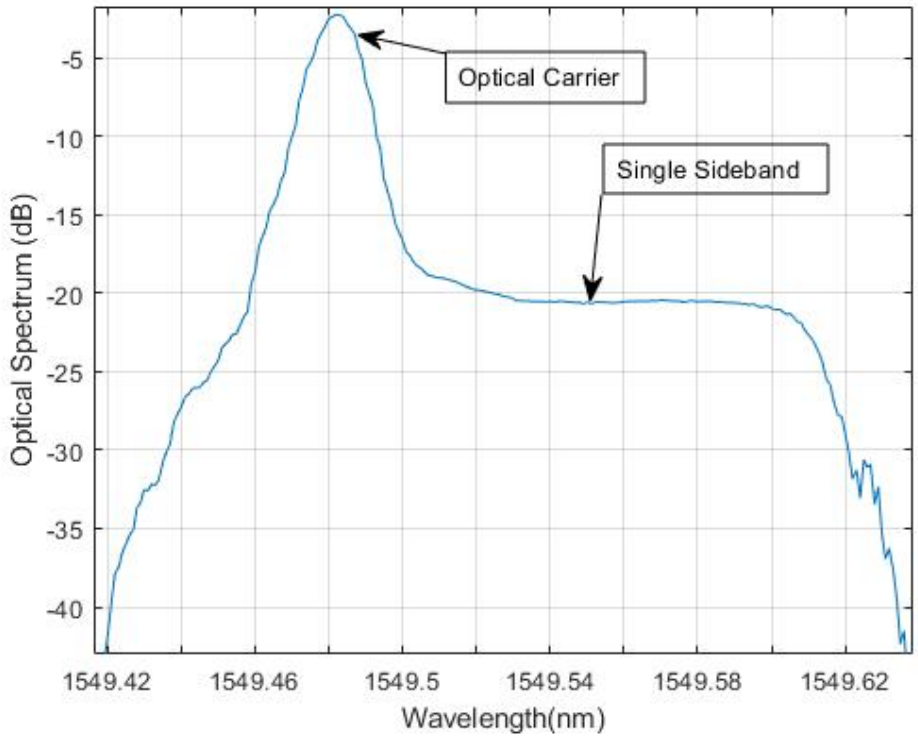

Figure 32: Single sideband modulated Optical Spectrum

The electrical signal at the photodiode output is pre-amplified and sampled by a real-time oscilloscope for analog-to-digital conversion (ADC) at 100GS/s sampling speed. The sampled signal waveform is processed in the digital domain to recover the original 14Gbaud QAM-16

signal with the data rate of 56Gb/s. Clock-recovery, KK phase reconstruction, dispersion compensation and demodulation are performed offline using Matlab. 107428 symbols (429712 total bits) were used for BER measurement. After photodetection of the signal, post-emphasis was performed digitally on the received signal to compensate for the roll off in the transfer function of the photo-detector. Figure 33 below shows the received RF spectrum of the 14G baud QAM 16 modulated signal after post-emphasis. In the receiver DSP, frequency response of receiver frontend was compensated, and the captured signal was re-sampled to 5 Sa/Symb. A DC component was then re-inserted to replace the DC component that was blocked by the AC-coupled RF amplifier.

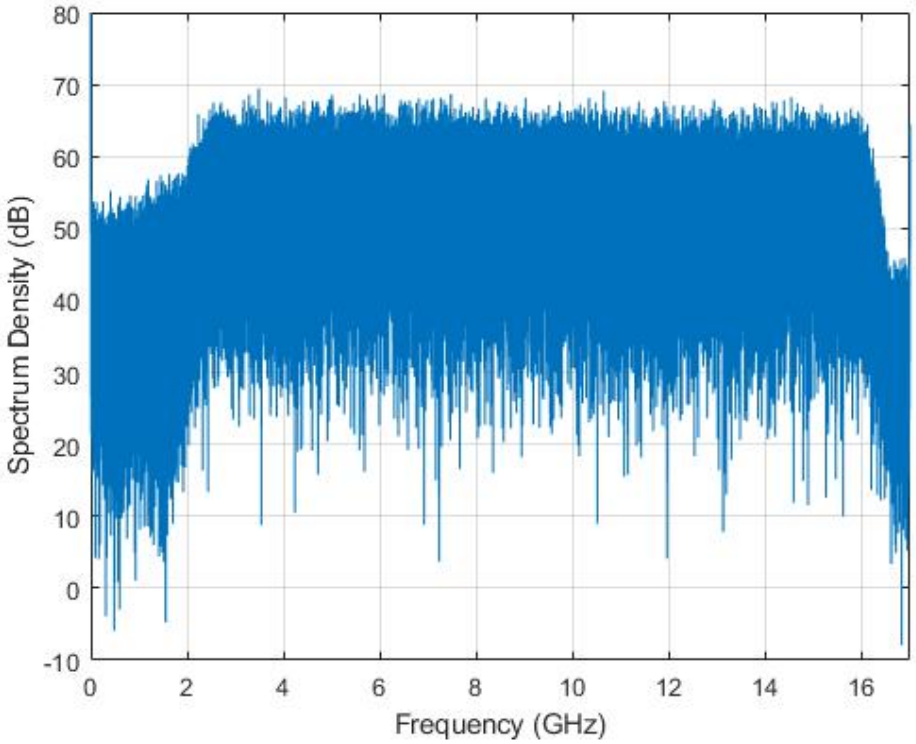

Figure 33: Received RF spectrum of 14G baud QAM16 signal

After KK field reconstruction and down-sampling to 2 Sa/Symb, frequency-domain dispersion compensation is applied to remove the impact of the fiber CD. This is followed by the down-conversion of the complex QAM signal center frequency to zero, matched filtering, clock recovery, 43-tap *T*-spaced adaptive equalization to remove residual ISI, and carrier phase recovery

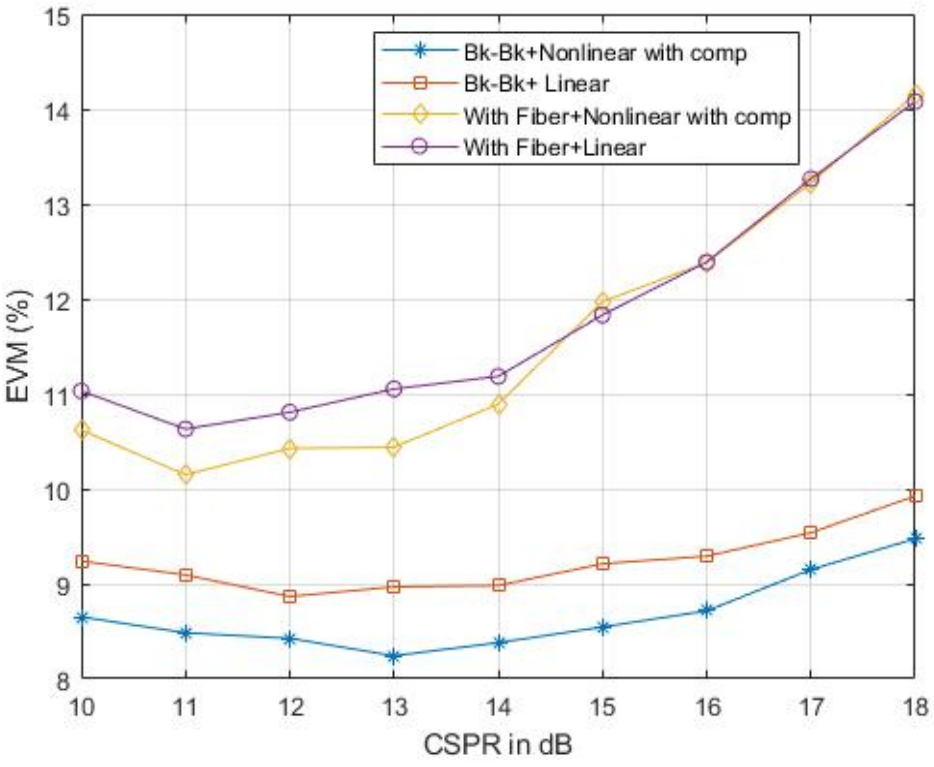

Figure 34:Experimental EVM vs CSPR plots for back to back setup and with fiber when SOA is operated in linear region (line with stars, line with squares) and nonlinear region with pre-compensation (line with diamonds, line with circles)

based on the blind phase search before symbol-to-bit hard decision de-mapping. The number of taps used for the adaptive equalizer was optimized to accommodate the relatively high ripple in the receiver transfer function

4.5 Experimental Results and Discussion

The effect of SSBI on the received signal is determined by CSPR. Higher the value of CSPR, lower the effect of SSBI. However, we cannot constantly increase the CW power to achieve higher CSPR. This is because, as we increase CW power the required OSNR of the signal would degrade leading to poor performance. We used performance metric error vector magnitude (EVM) which describes the effective distance of the received complex symbol from its ideal position in the constellation diagram [59]. This is a reliable measure for advanced modulated optical signals. To determine optimum CSPR for KK detection in our experimental setup we collected EVM versus

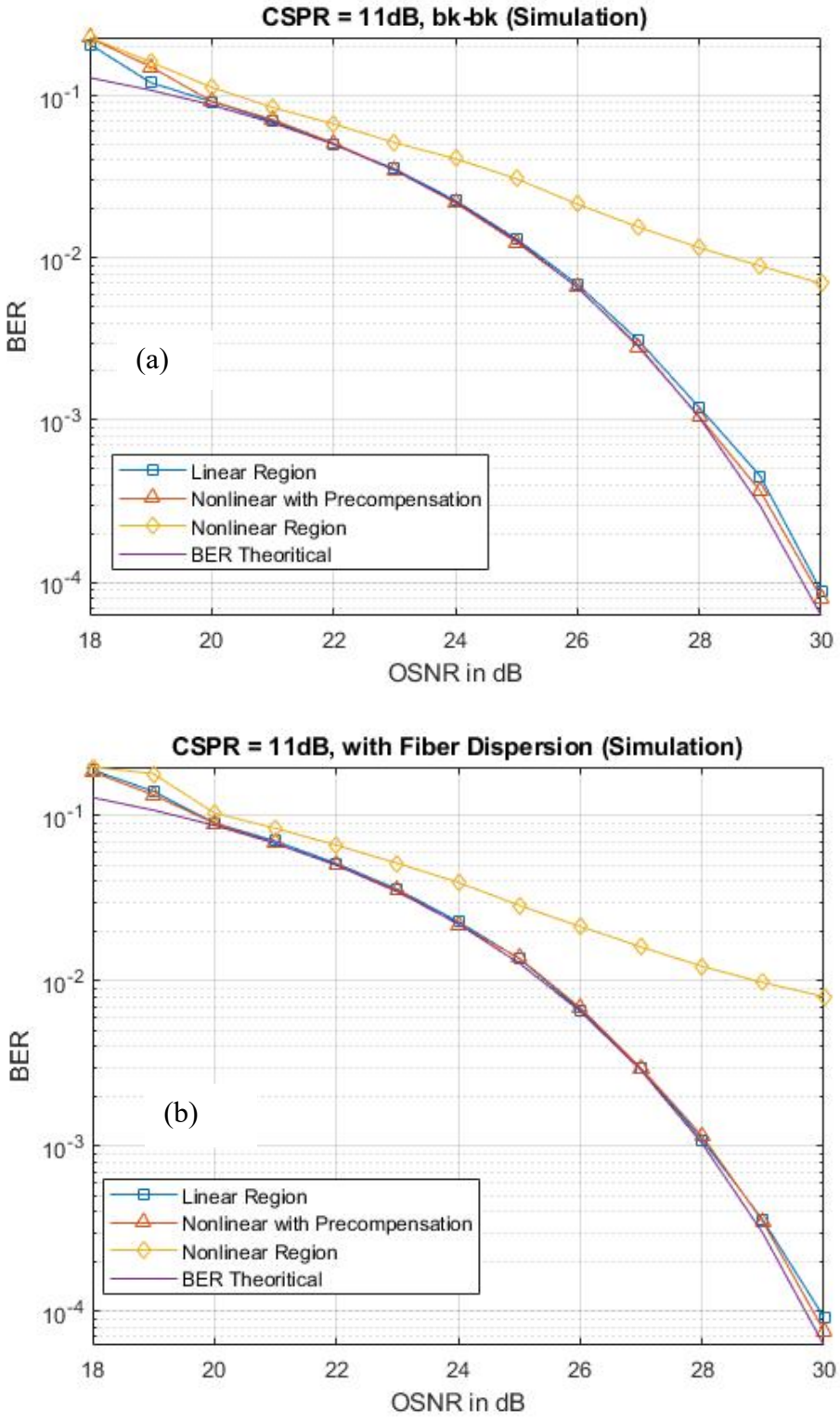

Figure 35:(a) and (b) shows simulation results of BER versus OSNR for back to back and with fiber dispersion

CSPR measurements in following scenarios: (a) when input optical power to SOA was set to -18dBm, to operate in linear region, (b) when input optical power to SOA was set to -8dBm, to

drive SOA into nonlinear region but pre-compensated for impairments. Both cases were tested on a back-to back setup at OSNRs of 44dB and 42dB. When with fiber at an OSNR of 40dB. The difference in OSNR was due to the noise added by EDFA which is used to amplify the signal as there is additional attenuation loss due to optical fiber.

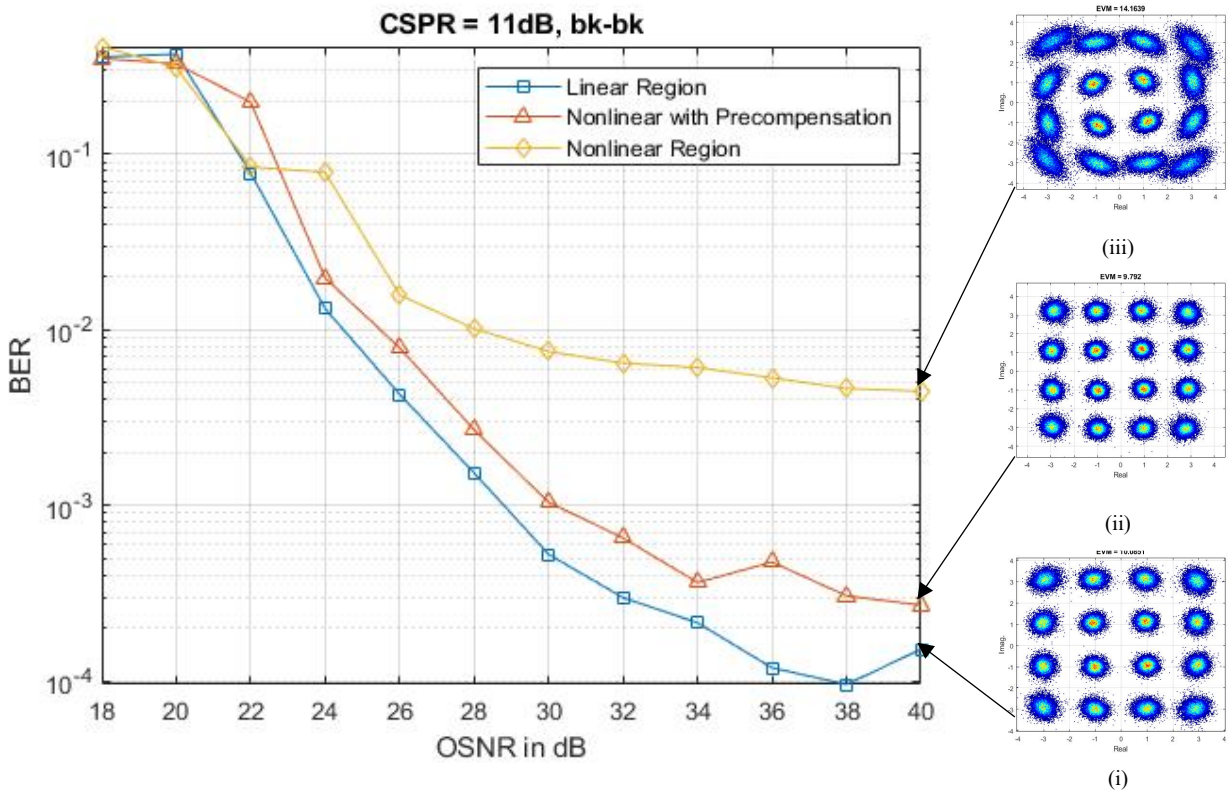

Figure 36:Experimental data showing BER Vs OSNR plots for back to back setup. CSPR of 11dB. Insets (i), (ii), (iii) shows typical constellation diagram of received QAM-16 signal when SOA is operated in linear region, nonlinear region with and without pre-compensation for impairments respectively

The Figure 34 shows the metric EVM in percentage as a function of CSPR in dB. The plots in Figures 35-37 shows measurements of BER as a function of OSNR. Figures 36 and 37 show experiment measurements. Figure 35 with insets (a) and (b) shows simulation calculations of the same. We performed simulation calculation of BER to check the validity of the idea of pre-compensating SOA induced nonlinearity in field modulation direct detection system in presence of fiber dispersion. Then we verified our idea experimentally.

To achieve good phase recovery using KK receiver in presence of fiber we used CSPR of 11dB in our experiments to measure BER. In all plots of BER vs OSNR we measured 3 scenarios based on how the SOA is operated. They're (a) when SOA is operated in linear region, (b) when SOA is operated in nonlinear region without pre-compensation for impairments and (c) when SOA is operated in nonlinear region with pre-compensation for impairments. Insets (i), (ii), (iii) in Figure 36 shows typical constellation diagram for received QAM-16 signal when SOA is operated in 3 cases mentioned above.

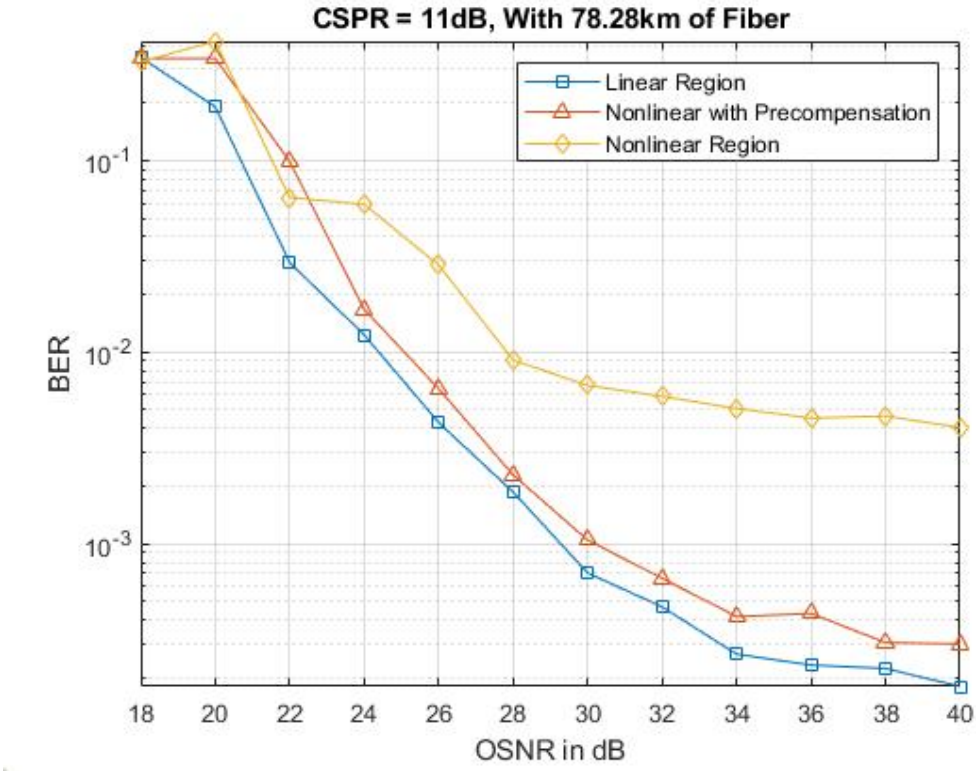

Figure 37:Experimental data showing BER vs OSNR for the case when 78.28km fiber was included. CSPR of 11dB

Consider Figure 36, that is measurements taken in back to back experimental setup. At an OSNR of 40dB and SOA is operated in linear region at a low input power of -18dBm, we can see that BER is in 10^{-4}s (line with squares). When SOA is driven by high input power of -8dBm, we can see that BER performance degrades for same OSNR and is in low 10^{-3}s (line with diamonds)

which is expected as SOA induces nonlinear impairments at this input power levels. Now see the plot (line with triangles), that is when SOA is operated in nonlinear region with pre-compensation for impairments done at transmitter, shows significant improvement. BER performance is almost same as when SOA is operated in linear region at OSNR of 40dB. Likewise, we can see similar results in the presence of fiber, shown in Figure 37. BER of 10^{-4}s when SOA is operated in linear region, 10^{-3}s when SOA is operated in nonlinear region, recovered BER performance when SOA induced nonlinearity is pre-compensated. We compensated for fiber chromatic dispersion post KK detection. As the SOA induced nonlinearities were pre-compensated, KK receiver efficiently recovers the phase information which in turn enables electronic dispersion compensation in direct detection system.

4.6 Conclusions

In this chapter, we have successfully demonstrated, a compensation method to mitigate SOA nonlinearity impairments when operated in gain saturation for field modulation direct detection system in the presence of fiber chromatic dispersion. The compensation for impairments induced by SOA was done using backpropagation method at transmitter side. We were also able to effectively implement receiver side EDC after KK receiver when SOA was operated in nonlinear regime. To the best of our knowledge this investigation is first experimental evaluation to compensate the effect of SOA induced nonlinearities in a field modulated direct detection transmission system.

Future Work

Improving resource requirement in DSP design for FPGA/ASIC realization, compensating nonlinearities due to SOA gain saturation in a Complex Field Modulated Direct Detection System was the main focus of this dissertation. We first investigated how to use low speed electronics such as DACs and ADCs to transmit and receive wide band signals using DSCM system. Then we researched how to reduce FPGA resources required for implementation of filters DSCM system with 2bits/s/Hz spectral efficiency while achieving no inter channel cross-talk and no inter-symbol interference. Lastly, we investigated a compensation method to mitigate SOA nonlinearities in a field modulated direct detection system with Kramers-Kronig phase recovery which effectively mitigates signal-signal beat interference as well. This also allowed us to achieve post electronic dispersion compensation in direct detection system.

In extension to already established research work, following are some potential research work that can be conducted:

1. Real time implementation of the Quadrature Duobinary modulation scheme on a resource constrained real-time hardware platform like FPGA evaluation board. This is important as it is crucial to validate the proposed DSP ideas.
2. Also, there is a good opportunity to study Kramers-Kronig receiver which is one of the hot topics in the field focused on direct detection. As this algorithm helps recover phase information from intensity detection.

REFERENCES

[1] D. Medhi, *Network Routing: Algorithms, Protocols, and Architectures*, 1st Edition, Morgan Kaufmann Publishing, 2007.

[2] James Macfarlane, Network Routing Basics: Understanding IP Routing in Cisco Systems, John Wiley & Sons, 2006.

[3] K. Nosu, *Optical FDM Network Technologies*, Artech House Publishers, 1997.

[4] W. Huang, et. al, "Digital Subcarrier Optical Networks (DSONs)", *Proc. ICTON* 2012.

[5] M. Jinno and e. al, "Spectrum-Efficient and Scalable Elastic Optical Path Network: Architecture, Benefits, and Enabling Technologies," *IEEE Communications Magazine*, pp. 66-73, November, 2009.

[6] K. Christodoulopoulos, I. Tomkos, and E. A. Varvarigos, "Elastic Bandwidth Allocation in Flexible OFDM Based Optical Networks," *J. Lightwave Technol.* 29(9), 1354–1366 (2011).

[7] Y. Zhang, M. O'Sullivan, and R. Hui, "Digital subcarrier multiplexing for flexible spectral allocation in optical transport network" *Optics Express*, Vol. 19, No. 22, pp. 21880-21889, 2011.

[8] P. Bower and I. Dedic, " High speed converters and DSP for 100G and beyond," *Optical Fiber Technology*, Vol. 17, pp. 464–471, 2011.

[9] R. Hui, B. Zhu, R. Huang, C. Allen, K. Demarest, and D. Richards, "Subcarrier multiplexing for high-speed optical transmission," *J. Lightwave Technol*., Vol. 20, No. 3, pp. 417 –427, 2002.

[10] F. A. Guti´errez, P. Perry, E. P. Martin, A. D. Ellis, F. Smyth, and L. P. Barry, "All-Analogue Real-Time Broadband Filter Bank Multicarrier Optical Communications System," *J. Lightwave Technol*., Vol. 33, 2015.

[11] F. Idzikowski, S. Orlowski, C. Raack, H. Woesner and A. Wolisz, "Saving energy in IP-over-WDM networks by switching off line cards in low-demand scenarios," in *Conference on Optical Network Design and Modeling (ONDM'10)*, Kyoto, Japan, Feb. 2010.

[12] A. Lowery and J. Armstrong, "Orthogonal-frequency-division multiplexing for dispersion compensation of long-haul optical systems," *Optics Express*, Vol. 14, No. 6, pp. 2079–2084, 2006.

[13] W. Shieh, H. Bao, and Y. Tang, "Coherent optical OFDM: theory and design*," Opt. Express Vol*. 16, pp. 841–859, 2008.

[14] G. Bosco, A. Carena, V. Curri, P. Poggiolini, and F. Forghieri, "Performance Limites of Nyquist-WDM and COOFDM in High-Speed PM-QPSK Systems," *IEEE Photon. Technol. Lett.*, Vol. 22, No.15, pp. 1129–1131, 2010.

[15] R. Schmogrow, et. al, "Real-time Nyquist pulse generation beyond 100 Gbit/s and its relation to OFDM," *Optics Express*, Vol. 20, pp. 317-337, 2012.

[16] Z. Xu, R. Hui and M. O'Sullivan, "Dual-band OOFDM system based on tandem single-sideband modulation transmitter" *Optics Express*, Vol. 17, Issue 16, pp. 13479-13486, 2009.

[17] A. J. Viterbi and A. M. Viterbi, "Non-linear estimation of PSK-modulated carrier phase with application to burst digital transmission," *IEEE Trans. Inf. Theory*, Vol. 29, pp. 543–551, 1983.

[18] R. Schmogrow, et. al, "Error Vector Magnitude as a Performance Measure for Advanced Modulation Formats," *IEEE Photonic Technology Letters*, Vol. 24, pp.61-63, 2012

[19] R. Hui and M. O'Sullivan, *Fiber Optic Measurement Techniques* (Chapter 5), Academic Press, 2009.

[20] A. Lender "The duobinary technique for high-speed data transmission" *IEEE Trans. Commun. Electron*. vol. CE-82 no. 66 pp. 214-218 May 1963.

[21] I. Lyubomirsky, "Quadrature Duobinary for High-Spectral Efficiency 100G Transmission," in *Journal of Lightwave Technology*, vol. 28, no. 1, pp. 91-96, Jan.1, 2010.

[22] J. G. Proakis M. Salehi Communication Systems Engineering NJ Englewood Cliffs:Prentice-Hall 1994.

[23] S. Walklin and J. Conradi, "Multilevel signaling for increasing the reach of 10 Gb/s lightwave systems," in *Journal of Lightwave Technology*, vol. 17, no. 11, pp. 2235-2248, Nov 1999.

[24] J. Li Z. Tao H. Zhang W. Yan T. Hoshida J. C. Rasmussen *J. Lightw. Technol.* vol. 29 pp. 1098-1104 2011.

[25] C. Xie and S. Chen, "Quadrature duobinary modulation and detection," *2015 Optical Fiber Communications Conference and Exhibition (OFC),* Los Angeles, CA, 2015, pp. 1-3.

[26] Rabiner, L. R. and Gold, B.: Theory and Application of Digital Signal Processing. Prentice-Hall Inc., 1975.

[27] Y. Zhang, M. O'Sullivan, and R. Hui, "Digital subcarrier multiplexing for flexible spectral allocation in optical transport network" *Optics Express,* Vol. 19, No. 22, pp. 21880-21889, October, 2011.

[28] S. Zhang, F. Yaman, L. Xu, Y. Shao and M. Cvijetic, "Pulse shaping on quadrature duobinary format," 2011 *IEEE Photonics Society Summer Topical Meeting Series*, Montreal, QC, 2011, pp. 149-150.

[29] J. Zhang, B. Huang and X. Li, "Improved Quadrature Duobinary System Performance Using Multi-Modulus Equalization," in *IEEE Photonics Technology Letters*, vol. 25, no. 16, pp. 1630-1633, Aug.15, 2013.

[30] S. Zhang, D. Chang, O. A. Dobre, O. Omomukuyo, X. Lin and R. Venkatesan, "Training Symbol-Based Equalization for Quadrature Duobinary PDM-FTN Systems," in *IEEE Photonics Technology Letters*, vol. 29, no. 5, pp. 454-457, March1, 1 2017.

[31] J. Zhang, J. Yu, Z. Dong, N. Chi and X. Li, "Multi-modulus blind equalizations for coherent spectrum shaped polmux quadrature duobinary signal processing," *2013 Optical Fiber Communication Conference and Exposition and the National Fiber Optic Engineers Conference (OFC/NFOEC)*, Anaheim, CA, 2013, pp. 1-3.

[32] K. Kaje and R. Hui, "Quadrature Duobinary Modulation and Detection Achieving 2Bit/s/Hz Spectral Efficiency to Reduce DSP Resource Requirement," *2018 IEEE International Conference on Communications Workshops (ICC Workshops)*, Kansas City, MO, 2018, pp. 1-6.

[33] R. Hui, K. Kaje and A. Fumagalli, "Digital-analog hybrid SCM for fine-granularity circuit-switched optical networks," *2016 18th International Conference on Transparent Optical Networks (ICTON)*, Trento, 2016, pp. 1-7.

[34] G. D. Forney, “Maximum-likelihood sequence estimation of digital sequences in the presence of intersymbol interference,” *IEEE Trans. Commun.*, vol. 18, no. 3, pp. 363–378, May 1972.

[35] O. E. Agazzi, M. R. Hueda, H. S. Carrer and D. E. Crivelli, "Maximum-likelihood sequence estimation in dispersive optical channels," in *Journal of Lightwave Technology*, vol. 23, no. 2, pp. 749-763, Feb. 2005.

[36] D. Marcuse, “Calculation of bit-error probability for a lightwave system with optical amplifiers and post-detection Gaussian noise,” *J. Lightw. Technol.*, vol. 9, pp. 505–513, Apr. 1991.

[37] P. A. Humblet and M. Azizoglu, “On the bit error rate of lightwave systems with optical amplifiers,” *J. Lightw. Technol.*, vol. 9, pp. 1576–1582, Nov. 1991.

[38] Antonio Mecozzi, Cristian Antonelli, and Mark Shtaif, "Kramers–Kronig coherent receiver," *Optica 3*, 1220-1227 (2016)

[39] C. Sun, D. Che, and W. Shieh, "Comparison of Chromatic Dispersion Sensitivity between Kramers-Kronig and SSBI Iterative Cancellation Receiver," in *Optical Fiber Communication Conference*, OSA Technical Digest (online) (Optical Society of America, 2018), paper W4E.4.

[40] Available: https://www.cisco.com/c/en/us/solutions/collateral/executive-perspectives/annual-internet-report/white-paper-c11-741490.html

[41] G.D. Forney, Jr., ‘‘The Viterbi algorithm,’’ *Proc. IEEE,* vol. 61, pp. 268--278, Mar. 1973.

[42] H.M. Bae, J.B. Ashbrook, J. Park, N.R. Shanbhag, A.C. Singer, and S. Chopra, “An MLSE Receiver for Electronic Dispersion Compensation of OC-192 Fiber Links,” *IEEE J. Solid-State Circuits*, vol. 41, pp. 2541í2554, Dec. 2006

[43] J.P. Elbers, H. Wernz, H. Griesser, C. Glingener, A. Faerbert, S. Langenbach, N. Stojanovic, C. Dorschky, T. Kupfer, and C. Schulien, ‘‘Measurement of the dispersion tolerance of optical duobinary with an MLSE-receiver at 10.7 Gb/s,’’ in *Proc. OFC*, Anaheim, Mar. 2005, paper OthJ4.

[44] H.F. Hauntein, K. Sticht, A. Dittrich, W. Sauer-Greff, and R. Urbansky, ‘‘Design of near optimum electrical equalizers for optical transmission in the presence of PMD,’’ in *Proc. OFC*, Anaheim, Mar. 2001, pp.WAA4--1--WAA4--3.

[45] Zhengxuan Li, Lilin Yi, Xiaodong Wang, and Weisheng Hu, "28 Gb/s duobinary signal transmission over 40 km based on 10 GHz DML and PIN for 100 Gb/s PON," *Opt. Express* 23, 20249-20256 (2015).

[46] Y. Kim, J. Lee, Y. Kim, and J. Jeong, “Evaluation of transmission performance in cost-effective optical duobinary transmission utilizing modulator’s bandwidth or low-pass filter implemented by a single capacitor,” *Opt. Fiber Technol*. 10(4), 312–324 (2004).

[47] D. van Veen, V. E. Houtsma, P. Winzer, and P. Vetter, “26-Gbps PON Transmission over 40-km using duobinary detection with a low cost 7-GHz APD-based receiver,” *in Proc. ECOC 2012*, paper Tu.3.B.1.

[48] T. Ono, Y. Yano, and K. Fukuchi, “Demonstration of high-dispersion tolerance of 20-Gbit/s optical duobinary signal generated by a low-pass filtering method,” *In Proc. OFC 1997*, paper ThH1.

[49] G. Katz, D. Sadot and J. Tabrikian, "Electrical Dispersion Compensation Equalizers in Optical Direct- and Coherent-Detection Systems," in *IEEE Transactions on Communications*, vol. 54, no. 11, pp. 2045-2050, Nov. 2006.

[50] Available:https://www.cisco.com/c/dam/m/en_us/solutions/service-provider/vni-forecast-highlights/pdf/Global_2022_Forecast_Highlights.pdf

[51] M. A. Hameed, M. O’Sullivan and R. Hui, "Impact of SOA-induced nonlinear impairments in CO-OFDM and Nyquist sinc-pulse transmission", *Proc. Asia Commun. Photon. Conf.*, 2013.

[52] H. Khaleghi, A. Sharaiha, T. Rampone, P. Morel and M. Guegan, "Semiconductor optical amplifiers in coherent optical-OFDM systems", *IEEE Photon. Technol. Lett.*, vol. 24, no. 7, pp. 560-562, Apr. 2012.

[53] G. P. Agrawal and N. A. Olsson, "Self-phase modulation and spectral broadening of optical pulses in semiconductor laser amplifiers", *IEEE J. Quantum Electron.*, vol. 25, no. 11, pp. 2297-2306, Nov. 1989.

[54] X. Li and G. Li, "Electrical postcompensation of SOA impairments for fiber-optic transmission", *IEEE Photon. Technol. Lett.*, vol. 21, no. 9, pp. 581-583, May 2009.

[55] Z. Li *et al*., "SSBI Mitigation and the Kramers–Kronig Scheme in Single-Sideband Direct-Detection Transmission With Receiver-Based Electronic Dispersion Compensation," in *Journal of Lightwave Technology*, vol. 35, no. 10, pp. 1887-1893, 15 May15, 2017, doi: 10.1109/JLT.2017.2684298.

[56] A. Mecozzi, C. Antonelli and M. Shtaif, "Kramers-Kronig coherent receiver", *Optica*, vol. 3, no. 11, pp. 1220-1227, 2016.

[57] R. I. Killey, P. M. Watts, V. Mikhailov, M. Glick and P. Bayvel, "Electronic dispersion compensation by signal predistortion using digital processing and a dual-drive Mach-Zehnder modulator", *IEEE Photon. Technol. Lett.*, vol. 17, no. 3, pp. 714-716, Mar. 2005.

[58] G. Vedala, M. A. Hameed and R. Hui, "Digital Compensation of SSBI in Direct Detection Multicarrier System with SOA Nonlinearities," in *IEEE Photonics Technology Letters*, vol. 29, no. 4, pp. 369-372, 15 Feb.15, 2017, doi: 10.1109/LPT.2016.2647561

[59] R. Schmogrow et al., "Error Vector Magnitude as a Performance Measure for Advanced Modulation Formats," in *IEEE Photonics Technology Letters*, vol. 24, no. 1, pp. 61-63, Jan.1, 2012, doi: 10.1109/LPT.2011.2172405.

[60] I. Tomkos, et al, "A tutorial on the flexible optical networking paradigm: State of the art, trends, and research challenges," in *Proceedings of the IEEE*, vol. 102, no. 9, pp. 1317-1337, Sept. 2014.

[61] M. Imran, P. M. Anandarajah, A. Kaszubowska-Anandarajah, N. Sambo and L. Potí, "A Survey of Optical Carrier Generation Techniques for Terabit Capacity Elastic Optical

Networks," in *IEEE Communications Surveys & Tutorials*, vol. 20, no. 1, pp. 211-263, Firstquarter 2018, doi: 10.1109/COMST.2017.2775039.